Modelling of loss factors of elastomer binders of high explosive charges and composite rocket propellants used to follow ageing

Manfred A. Bohn

Fraunhofer Institut fuer Chemische Technologie (ICT) D-76318 Pfinztal Germany

Manfred.Bohn@ict.fraunhofer.de

Abstract

In the temperature range of the loss factor tanδ = G''/G' = E''/E' determined by DMA (dynamic mechanical analysis) the transition from the energy elastic to the entropy elastic behavior, or vice versa, occurs. This phenomenon is often called glass transition but better named glass-rubber transition. The binder has several fractions with different molecular mobility caused by interaction between polymer chains and fillers. This leads to different transition regions, which change in intensity differently by external impacts as deformation rate and aging. A peak separation of the loss factor curve is necessary to determine the influence of such external impacts on the sample. This is achieved by: (i) baseline correction of the loss factor curve to separate most of the dissipative parts; (ii) modeling of the baseline corrected loss factor to quantify the different elastomer mobility fractions. The separation of the dissipative part in the loss factor curve is done by an iterative baseline correction function, using a transient function, which is a cumulative partition variable, to adjust the baseline weights along the loss factor curve.

After the baseline correction a suitable fit function must be chosen in order to evaluate the areas under the peaks of the loss factor curve. If the values of the interaction energies and the molecular docking regions are randomly distributed in the isotropic material, a Gauss distribution should describe the processes. Mostly the shapes of the loss factor curves are not symmetrical, meaning that some dissipative parts are still present, which can be described with relaxation curves represented with exponentially decreasing functions. The combined processes result in an exponentially modified Gauss distribution function (EMG).

Three EMGs have been applied to loss factor curves of composite rocket propellant, which allowed to identify three mobility ranges. The description of the data is very good. The main changes with ageing or deformation rate are not in the dominant peak or main transition of the mobility unrestricted elastomer fraction but in the two other molecular reorientation regions, where the elastomer is mobility restricted in different ways by interaction with filler particles and by the curing agent. Therefore these parts can be used as aging indicator for composite rocket propellants and polymer bonded high explosive charges.

Keywords: dynamic mechanical analysis; glass-rubber transition; modelling of loss factor; exponentially modified Gauss distribution; separation of binder fractions with different mobility.

1 The loss factor and its meaning

The loss factor is best determined with DMA measurements, in principle in any measurement mode as torsion, tension, bending (single and dual cantilever), shear and compression in selected cases. For elastomers highly filled with rigid particles as composite rocket propellants and PBX (plastic bonded explosives) materials, the torsion mode seems to be the most suitable one. The measurement conditions for this mode can be found in [1]. The specimens are tested at several deformation frequency values as 0.1, 1.0, 10, 30 Hz, 56 Hz, using a strain control in order to stay in the so-named linear visco-elastic range domain, which means the modulus should be independent of the strain.

In torsion mode the measurement quantity is the dynamic torque M from which the complex shear modulus G* = τ*/γ* = G' + i G'' is calculated. G' is the storage shear modulus, G"

Paper on the NDIA - IM & EM Technology Symposium (IMEMTS), on 'IM & EM: Real Warfighter Advantage and Cost Effective Solutions Throughout the Lifecycle', 18-21 May 2015, Rome, Italy.

is the loss shear modulus, τ^* represents the complex shear stress and γ^* is the complex hear deformation. The loss factor $\tan\delta$ is defined in Eq. (1).

$$\tan\delta = \frac{G''}{G'} = \frac{E''}{E'} = \frac{J''}{J'} = \frac{\eta'}{\eta''} \qquad (1)$$

It is the ratio between loss modulus G'' or E'' and storage modulus G' or E' or, equivalently, the definition with loss and storage compliance J or with the complex viscosity, whereby $\eta'=G''/\omega$ and $\eta''=G'/\omega$. In a certain way the loss factor is the loss modulus normalized by the storage modulus. The angle δ is called the phase angle and describes the phase shift between the applied deformation phase and the phase registered from the instrument on the opposite side of the forced sample deformation. In terms of mechanical quantities it is the angle between stress and strain vectors. The loss factor region defines the region of glass-rubber transition and vice versa, which is often in short named glass transition, but this is somewhat inadequate, because there is also a glass-liquid transition, from which it should be distinguished. The glass-rubber transition always extends over a temperature region. It is mostly characterised by the temperature of the maximum in $\tan\delta$ or of several maxima in $\tan\delta$. However, as explained in this paper, it is better to use the areas and parameters of the sub-transition regions of the loss factor as characteristic quantities.

The glass-rubber transition is a temperature induced transition of an amorphous polymer phase from its energy elastic state to its entropy elastic state and vice versa. In other words, it is the region of the molecular rearrangements of the polymer molecules from their enthalpy dominated interaction to their entropy dominated state. Table 1 gives the basic composition of the three energetic materials discussed in this paper. All three have the same type of binder. The composite rocket propellant CRP1 uses a bonding agent for the ammonium perchlorate (AP) particles, which establishes primary (chemical) bonds to AP and to the binder. This creates around the AP particles a so-named rubbery shell, which is highly compact but not completely rigid, because this would give only reduced advantage. HEC HX1 uses no bonding agent. In HEC HX2 a bonding agent establishing only secondary (physical) bonds was applied.

Table 1: Basic composition of three energetic materials compared in this work.
Composition in mass-%.
HTPB: hydroxyl terminated polybutadiene
IPDI: isophorone diisocyanate (curing agent)
DOA: dioctyl adipate (plasticiser);
CRP: composite rocket propellant formulation
Al: aluminium powder AP: ammonium perchlorate
HEC: high explosive charge HX: high explosive,

material	binder	filler	plasticiser	others (small amounts added to binder)
HEC HX1	HTPB-R45M IPDI, 12 m.-%	RDX, 80 m.-%	DOA, 8 m.-%	antioxidant.
HEC HX2	HTPB-R45HTLO IPDI, 14 m.-%	HMX, 85 m.-%	DOA, 1 m.-%	antioxidant, bonding agent for HMX.
CRP1	HTPB-R45M IPDI, 12 m.-%	Al, 6 m.-% AP, 78 m.-%	DOA, 4 m.-%	antioxidant, bonding agent for AP, no burning catalyst for AP.

Fig. 1 shows the storage and loss shear moduli of HX1 material obtained by DMA in torsion mode at three deformation frequencies. In Fig. 2 the typical loss factor curves $\tan\delta=G''/G'$ of the HTPB-IPDI-based bonded material can be seen. The curves show clearly two maxima, both are deformation frequency dependent. The first maximum is located between -80°C and -40°C (depending on the applied deformation frequency); the second maximum is broader than the first one and appears at higher temperature values, between -50°C and +20°C.

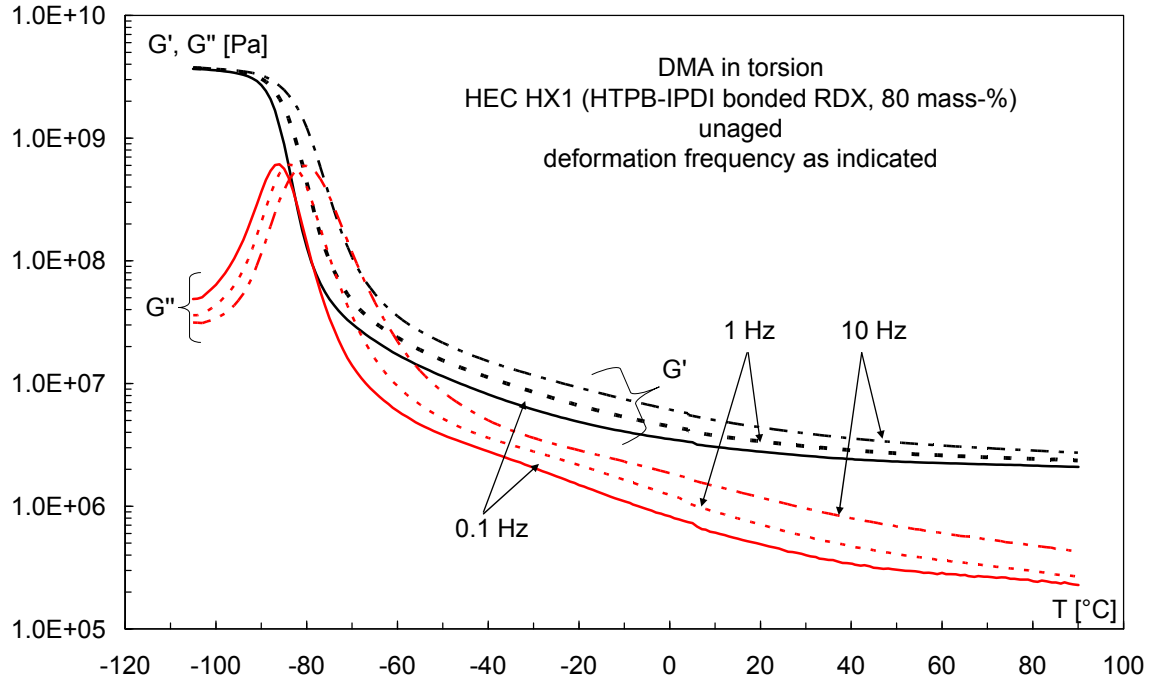

Figure 1: Storage shear modulus G' and loss shear modulus G'' of HEC HX1 vs. temperature at three deformation frequencies. The tensile moduli E' and E'' show the same type of curves.

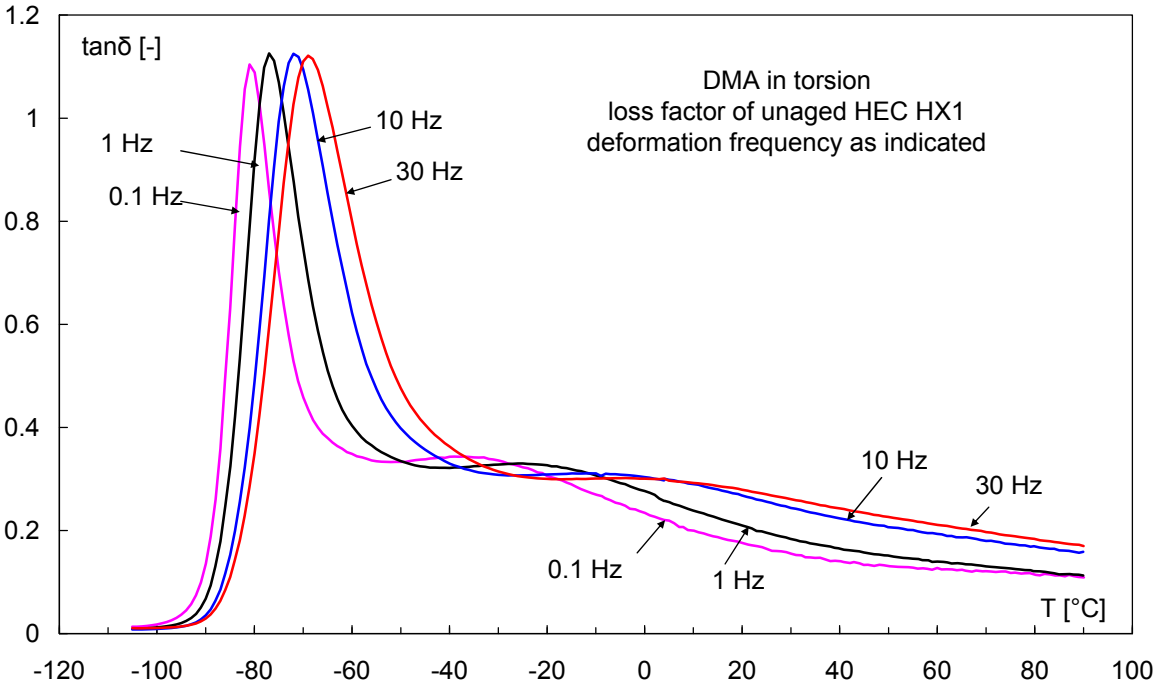

Figure 2: Loss factor tanδ vs. measurement temperature for HEC HX1. There are two evident maxima corresponding to two molecular rearrangement regions and processes.

In Fig. 3 the loss factor curve of the composite rocket propellant formulation CRP1 is shown. Principally the curves have the same features as the binder of the HEC HX1. Here the fillers are aluminium powder and ammonium perchlorate particles. The CRP1 belongs to the type of formulations described and investigated in [1, 2, 3, 4, 5]. It has no burning catalyst for AP, which is usually an iron compound as iron oxide (Fe_2O_3) or ferrocene (cyclopentadienyl iron) containing substances. It must be stated that these compounds foster the autoxidation of the HTPB binders by oxygen strongly. In Fig. 4 the baseline corrected (BLC) loss factor curves of the three considered formulations can be seen. All materials have the

same binder type and therefore the same basic structure in the loss factor curve. The meaning of the baseline correction is given in section 4.1.

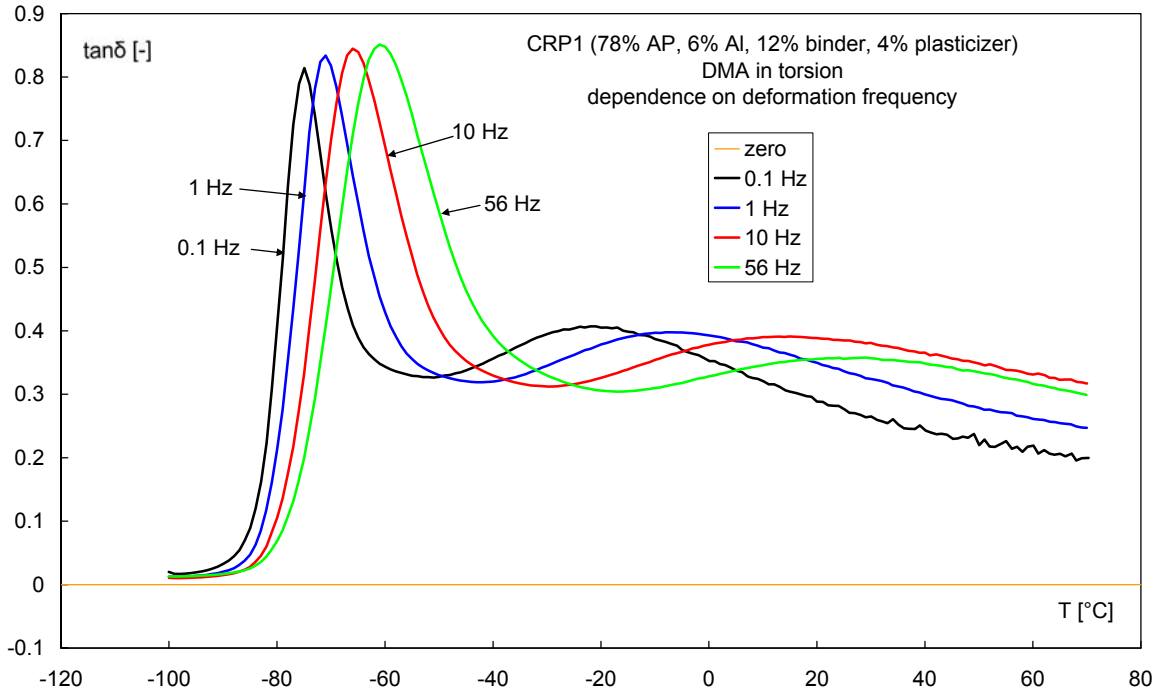

Figure 3: Loss factor tanδ vs. measurement temperature of CRP1, in which an active bonding agent for AP is used.

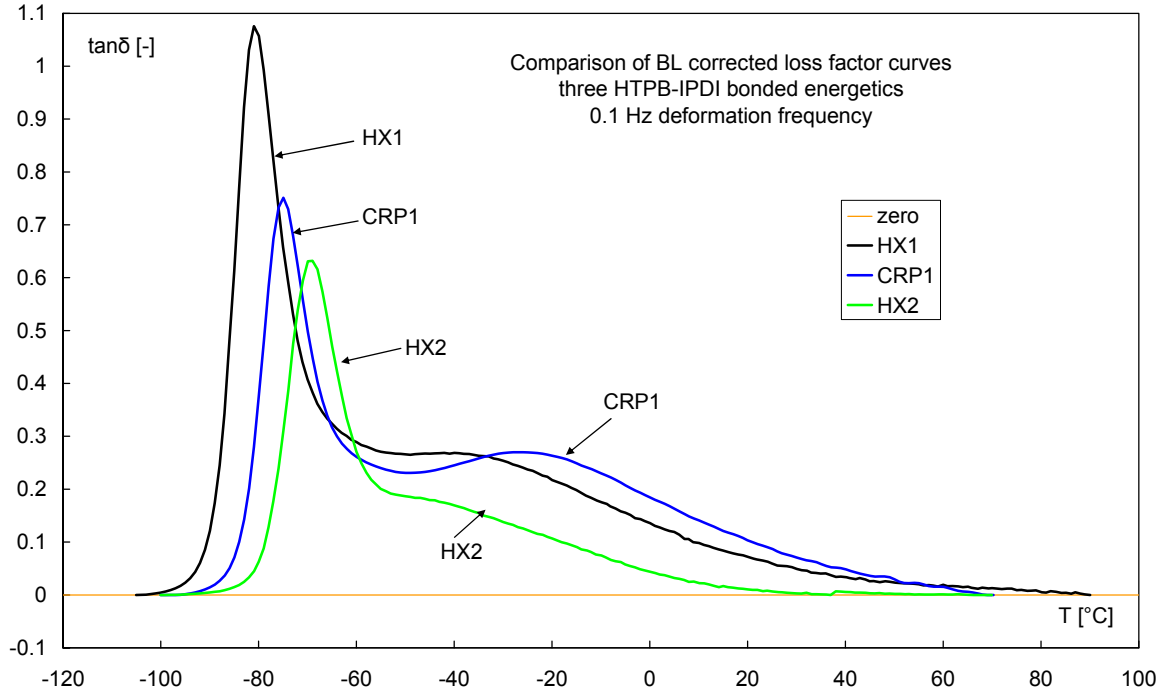

Figure 4: Baseline corrected loss factor tanδ vs. temperature for three energetic formulations made with the same type of binder, HTPB-IPDI. The basic structure of tanδ is the same for all three materials.

1.1 Glass transition temperature

What is the glass transition temperature? First we have to say that we consider here only the glass-rubber transition and not the glass-liquid transition or a glass-gel transition.

There are several definitions and argumentations for the glass transition temperature with elastomers, two of them are used mostly and discussed here. One group of people says the maximum of the loss modulus (G'' or E'') is the glass transition temperature. If one takes this value then the binder is already in a glassy state, which means that the free volume for the bigger chain segments of the elastomeric material is already so small that the polymer chains can no longer rearrange within the material. But the motions of these bigger chain segments caused by mechanical impact are responsible for the behaviour and the response of the material: brittle or (residual) ductile. If no free volume is available for those rearrangements, the material behaves in a brittle way. The consequence is the material may be damaged in the molecular structure on mechanical impact. Considering these implications, it is better to name the temperature value at the maximum of the loss modulus as **glass temperature and not glass transition temperature,** because the material is essentially in the glassy state with respect to rearrangement possibilities for bigger elastomer chain segments.

The second definition considers the glass-rubber transition temperature as the maximum of the loss factor curve of the elastomer. At the maximum intensity of the loss factor the molecular rearrangement process from glassy to rubbery state and vice versa is at its maximum. For the elastomeric materials this is the essential process characterising the change from the energy elastic state (glass) to the entropy elastic state (rubber). Therefore, in order to characterise the transition between these two states, the temperature corresponding to the maximum of the loss factor $\tan\delta$ must be taken, which is then correctly named as glass-rubber transition temperature or rubber-glass transition temperature. In compact form the best way is to name it glass-rubber transition temperature.

It must be noted that the loss factor is much more informative than the loss modulus in showing clearly the different temperature regions of the molecular rearrangements. Especially with HTPB-IPDI binders two apparent maxima can be found. Both are equally important for assessing the properties of the material and its behaviour under load.

1.2 Principle temperature behaviour of an elastomer

Polymers, especially weakly cross-linked elastomers as the binders of CRP1 propellant and HEC, change from a glass-like to rubber-like behaviour by increasing temperature. In the glassy state, at low temperature, the behaviour is related to the changes in the stored elastic energy by small displacements of the molecules from their equilibrium positions. In the rubbery state, at high temperatures, the molecular chains have much more accessible free volume and can adopt a large number of conformations, which leads to an increase in entropy. Here the alignment of the chains by any tensile forces or others reduces the entropy and the molecular reformation (also called relaxation) of the chains to their maximum entropy condition is the driving force and results in rubber elasticity. Scanning the temperature from one state region to the other, the material passes through an in-between region, where transitions occur as change in molecular arrangements. Generally this phenomenon is named glass-rubber transition region. The loss factor gives the normalized part of the applied deformation energy, which is consumed by the sample. The other part is transported elastically (means here loss free) through the sample and reaches the response detector. $\tan\delta = 0$ ($\delta = 0°$) means only elastic deformation takes place and with $\tan\delta = > 10$ considerable viscoelastic effects consume energy. At $\delta = 90°$ ($\tan\delta = \infty$) the materials is only viscous like a liquid.

The driving force for this temperature induced transition, from energy elastic to its entropy elastic state und vice versa, is to reach the lowest internal energy. When the variables controllable by the experiment are pressure, temperature and material amount (PTN) this quantity is the Gibbs free energy (also Gibbs free enthalpy in non Anglo-Saxon literature), Eq.(2).

$$\Delta G(p,T) = \Delta H(p,T) - T \cdot \Delta S(p,T) \qquad (2)$$

In the energy elastic state the internal energy is controlled by lattice like energetic interactions between the polymer molecules. The enthalpy term ΔH controls the Gibbs free energy ΔG. Because at lower temperatures the distances between the polymer chain elements are small, mobility is restricted and local dipole-dipole interactions have a strong effect in lowering the internal energy, so ΔH becomes appreciably negative. The entropy term plays nearly no role, because there is little change in configuration and conformation of the polymer chains. In the entropy elastic state the internal energy is not controlled by lattice like energetic interactions between the polymer molecules. The rearrangement of polymer molecules, because of more free volume available at higher temperatures, gives them the possibility to form many configurations, means that entropy is increased, the term $T \cdot \Delta S$ gets more positive, but ΔG gets more negative. Therefore, the entropy term $T \cdot \Delta S$ controls now the ΔG. ΔH increases, means is less negative than in energy elastic state. It plays now nearly no role, because its value varies only little in changing the conformations of the binder chains. The cause is that the distances between the chain elements have increased. Local dipole-dipole-interactions are less effective because of the motions of the chain elements, which average this interaction down to small values [6]. Even the interaction between permanent dipole – permanent dipole are averaged statistically over thermal energy determined orientations and finally this interaction has a dependence on distance by $1/r^6$, see Eq.(3). But at lower temperatures, when the permanent dipoles catch each other, Eq.(4) is valid and the interaction has a $1/r^3$ dependence.

$$V(r) = -2 \cdot \left(\frac{p_1 \cdot p_2}{4\pi\varepsilon_0} \right)^2 \cdot \frac{1}{3 \cdot kT} \cdot \frac{1}{r^6} \tag{3}$$

$$V(r) = -\frac{p_1 \cdot p_2}{(4\pi\varepsilon_0)} \cdot \frac{1}{r^3} \left(2\cos\theta_1 \cos\theta_2 - \sin\theta_1 \sin\theta_2 \cos(\phi_2 - \phi_1) \right) \tag{4}$$

This effect can also be shown by molecular dynamics or atomistic simulations, as done in a recent paper on HTPB systems including a polar binder based on polypropylene glycol [7, 8]. Any effect that reduces the possibility of realisation of polymer chain configurations will reduce the entropy part and makes the material less entropy elastic. In a not too large deformed state the polymer chains can adopt many conformations, which lead to a maximum of entropy. But this is no longer the case at strong compression or strong elongation; also for situations well above the glass-rubber transition temperature. In such cases the free volume is reduced and the polymer network gets more rigid and the glass-rubber transition intensity is reduced or even disappears. The network can be transformed mechanically from a so-named mobile amorphous phase (MAP) to a rigid amorphous phase (RAP), which in the end is not able to show a glass-rubber transition. This means it no longer transforms to the entropy elastic state. Because only parts of the network are normally involved, the expression mobile amorphous fraction (MAF) and rigid amorphous fraction (RAF) are applied also. The interaction of fillers with the polymer matrix may be so strong that RAF regions can occur, especially with active fillers or fillers connected via bonding agents to the matrix.

Note: The pre-straining plays also a role in real rocket motor systems with CRP. Stress situations occur at low temperatures and the network loses entropy elasticity. Therefore not only due to the increasing oxidative cross-linking the strain capability is reduced but also because of these pre-straining effects.

2 Typical glass-rubber transition temperatures of some binders determined by DMA

Glass-rubber transition temperatures can be determined also by differential scanning calorimetry (DSC) as the temperature of the half height in the step of the change of specific heat c_P during the transition, because the specific heat increases going from energy to en-

tropy elasticity. These values are always significantly lower than the ones determined by DMA. The reason is the 'static' determination by DSC, which means no mechanical deformation causing strain hardening is applied, neglecting the volume change by thermal expansion. By increasing the mechanical deformation rate, a pseudo increase in stiffness by inertia effects inside the material is caused. This leads to a shift to higher temperature values of the transition region. By increasing the deformation rate the material has less time to readjust the positions and orientations of molecular groups: coming from the low temperature side, the energy elastic behaviour is retained longer as the deformation rate gets higher.

Table 2: Typical glass-rubber transition temperatures defined as temperature of the main maximum of the loss factor curve, in part determined by DMA, in part estimation.

Elastomeric binder (without plasticiser)	**Tg [°C] by DMA at some deformation frequencies**		
	0.01 Hz	0.1 Hz	10 Hz
HTPB (R45 M) – IPDI	- 75	- 70	- 65
HTPB (R45 HT) – IPDI	- 70	- 65	- 60
GAP (diol) – N100	- 41	- 36	- 28
GAP (diol, triol) – BPS	- 25	- 20	- 12
Desmophene D2200 – N3400	- 35	- 30	- 22

Table 3: Temperatures at maxima in loss factor, loss modulus and temperature derivative of storage modulus of unaged HEC HX1.

Maximum type	**T_{max} [°C]**				**difference betw. 30Hz and 0.1 Hz**
	0.1 Hz	**1.0 Hz**	**10 Hz**	**30 Hz**	
tanδ_max1	-80.9	-77.0	-71.8	-69.0	11.9
G''	-86.3	-83.8	-80.4	-78.8	7.5
dG'/dT	-86.5	-84.3	-81.2	-79.5	7.0
tanδ_max2	-41.4	-29.6	-15.1	-10.3	31.1

Table 4: Temperatures at maxima in loss factor, loss modulus and temperature derivative of storage modulus of unaged HEC HX2. The determination of the second maximum tanδ_max2 was not well possible at 30 Hz.

Maximum type	**T_{max} [°C]**				**difference betw. 30Hz and 0.1 Hz**
	0.1 Hz	**1.0 Hz**	**10 Hz**	**30 Hz**	
tanδ_max1	-66.61	-62.56	-57.03	-51.75	14.86
G''	-72.1	-69.29	-65.86	-62.55	9.55
dG'/dT	-72.29	-70.11	-67.05	-63.81	8.48
tanδ_max2	-50.97	-43.73	-37.09	-	(13.88)

Table 5: Temperatures at maxima in loss factor, loss modulus and temperature derivative of storage modulus of unaged CRP1.

Maximum type	**T_{max} [°C]**				**difference betw. 30Hz and 0.1 Hz**
	0.1 Hz	**1.0 Hz**	**10 Hz**	**56 Hz**	
tanδ_max1	-74.9	-71.1	-65.8	-60.7	14.2
G''	-79.9	-77.1	-73.8	-70.8	9.1
dG'/dT	-80.1	-77.4	-74.3	-72.2	7.9
tanδ_max2	-21.8	-6.6	14.4	26.2	48.0

Therefore, DSC glass-rubber transition temperature values correspond to very low deformation rates in DMA, which means very low deformation frequencies in case of forced sinusoidal excitation. To compare DMA-Tg ($Tg_{,DMA}$) with DSC-Tg ($Tg_{,DSC}$), the deformation frequencies have to be in the range 0.001 Hz and smaller. Moreover, with DSC such rearrangement processes cannot be seen, which do not change the specific heat. Typical DMA-Tg values of cured and unfilled binders are compiled in Table 2. Rule of estimation for a DMA measurement: in the range 0.001 to 100 Hz every decade increase in deformation frequency leads to an increase of the glass-rubber transition temperature Tg by typically 4°C to 5°C. More precisely, the temperature corresponding to the maximum of the loss factor curve

changes nearly logarithmically with deformation frequency. The Tables 3, 4 and 5 list the temperature $T_{max}(\tan\delta)$ of the main maximum of the loss factor, the temperature $T_{max}(G'')$ of the loss modulus G'', the temperature $T_{max}(dG'/dT)$ of the derivative of storage modulus G' and the temperature of the second maximum in $\tan\delta$. The Figs. 5 and 6 show the maximum temperature as function of the natural logarithm of deformation frequency. The linear correlation seems good. Remarkable is that the change with frequency of the second apparent maximum in the loss factor is much higher than for the other three maximum temperatures. The maximum temperatures presented in Tables 2 to 5 can be taken for a parameterization of Arrhenius type with the deformation frequency according to Eq.(5). The results are listed in the Tables 6, 7 and 8.

$$f(T_{max}) = Z_f \cdot \exp\left(-\frac{Ea}{R \cdot T_{max}}\right) \qquad (5)$$

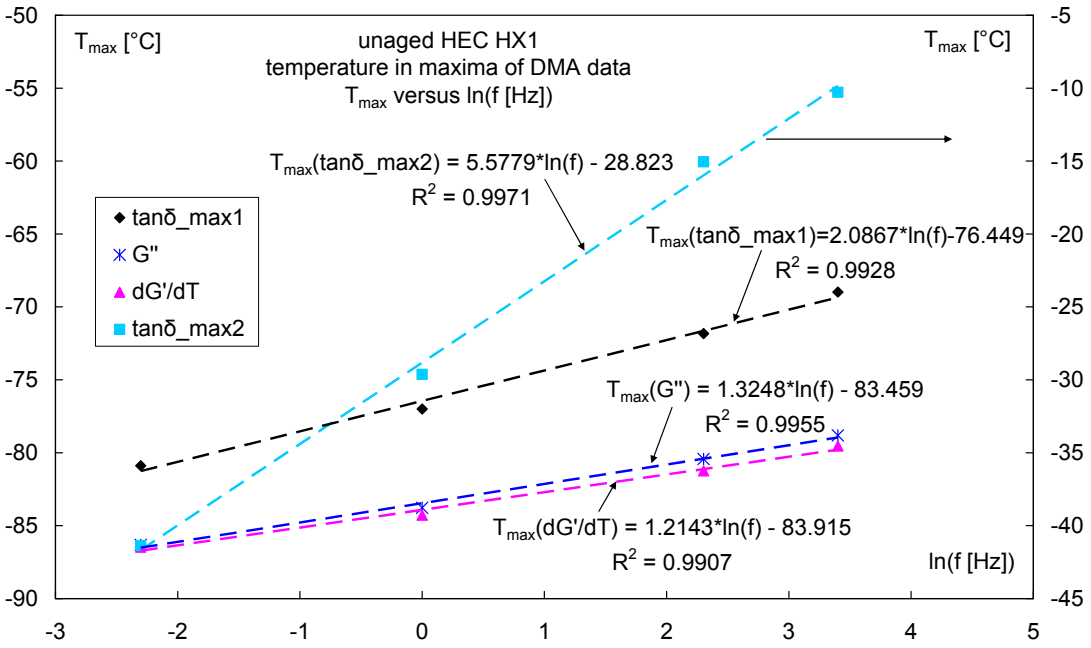

Figure 5: Temperatures at maxima in the DMA data of HEC HX1 as function of the natural logarithm of deformation frequency. The maximum temperature of the second loss factor peak has much higher frequency dependence than the other ones.

Noteworthy is the change in activation energies in going from the low temperature maxima to the high temperature maxima. The maximum temperatures of the loss modulus G'' is always connected with a quite high activation energy of about 225 to 230 kJ/mol, whereas the main maximum temperatures of the loss factor shows significantly lower values in the range 154 to 160 kJ/mol. The second maximum of loss factor gives apparent activation energies between 80 and 90 kJ/mol [4, 5, 6]. The interpretation of this trend is the change in intermolecular interaction energies [7]. At low temperatures the molecules have a smaller distance to neighbour molecules and the interaction energies are higher, also with only the vdW interactions, their values can be surprisingly high, see [8]. With increasing temperature the distances between the molecules increase and interaction energies decrease until the transition to entropy determined state happens. This course of the activation energies underlines the interpretation for the maximum of G'' as glass temperature and using the term glass-rubber transition temperature for the maxima of loss factor curve. At the maxima of G'' the material is already in the glassy state.

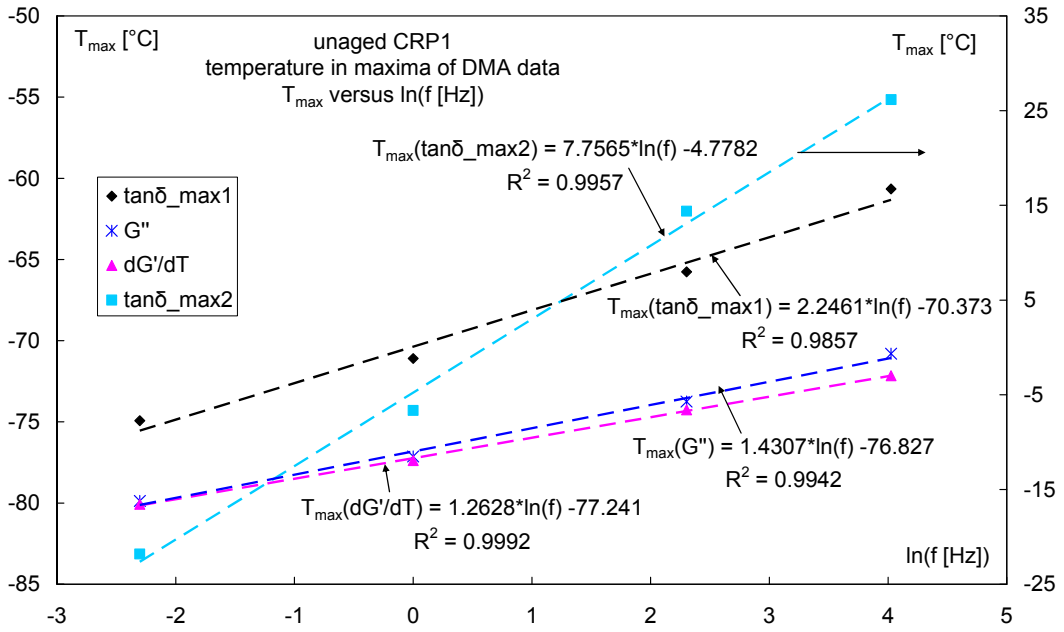

Figure 6: Temperatures at maxima in the DMA data of CPR1 as function of the natural logarithm of deformation frequency. The maximum temperature of the second loss factor peak has much higher frequency dependence than the other ones.

One important remark will be given here. Generally it is assumed that with some plasticiser all the problems with a too high glass-rubber transition can be solved. This is by far not true. It is even the case that the choice and applications of suitable plasticisers is limited and complex selection procedure must be used to find a good plasticiser for the special application in consideration. See the recent work reported in [9, 10]. Also the choice of the curing agent has a not neglectable influence on loss factor and also tensile strain properties [9, 10].

Table 6: Arrhenius type parameterisation of the maximum temperatures of HX1 with the deformation frequency.

type of maximum temperature	HEC HX1		
	Ea [kJ mol^{-1}]	lg(Z_f [Hz])	R^2
tanδ_max1	155.5 ± 8	41.304 ± 2.0	0.9952
tanδ_max2	90.6 ± 3.5	19.421 ± 0.7	0.9970
G"	227.0 ± 9	62.512 ± 2.5	0.9967
dG'/dT	245.4 ± 15	67.750 ± 4.2	0.9924
P1, Tc1	177.3 ± 11	47.395 ± 2.8	0.9929
P2, Tc2	161.1 ± 15	41.690 ± 3.9	0.9828
P3, Tc3	115.2 ± 11	26.464 ± 2.5	0.9815
P1, EMG	172.7 ± 9	45.961 ± 2.4	0.9945
P2, EMG	137.2 ± 10	34.707 ± 2.4	0.9904
P3, EMG	85.3 ± 5	17.854 ± 1.1	0.9926

Table 7: Arrhenius type parameterisation of the maximum temperatures of HX2 with the deformation frequency. The temperatures of the second maximum could not be determined well from the shape of the loss factor curve.

type of maximum temperature	HEC HX2		
	Ea [kJ mol^{-1}]	lg(Z_f [Hz])	R^2
tanδ_max1	160.8 ± 11	39.782 ± 2.7	0.9902
tanδ_max2	-	-	-
G"	233.2 ± 14	59.659 ± 3.5	0.9932
dG'/dT	258.5 ± 24	66.382 ± 6.2	0.9827

Table 8: Arrhenius type parameterisation of the maximum temperatures of CRP1 with the deformation frequency.

type maximum temperature	CRP1		
	Ea [kJ mol^{-1}]	lg(Z_f [Hz])	R^2
tanδ_max1	154.1 ± 11	39.711 ± 2.8	0.9899
tanδ_max2	80.3 ± 4	15.691 ± 0.7	0.9958
G''	226.2 ± 10	59.325 ± 2.7	0.9960
dG'/dT	255.3 ± 5	68.076 ± 1.2	0.9994

3 Modelling of loss factor curve to quantify mobility regions

3.1 Baseline correction of the loss factor curve

The deformation energy applied to the sample during the DMA measurements is in part transmitted loss free from the donor to the acceptor and in part used up by the sample, especially in the glass-rubber transition region. This second phenomenon has two contributions: a purely dissipative one in which the energy is transformed to heat by frictional effects, and a contribution used for the molecular rearrangements, which needs energy to separate the molecules. Energy is also necessary when going from the rubbery to the glassy state in order to reduce the entropy of the system. Outside the glass-rubber transition regions only dissipative consumptions occur, which are usually small, particularly in the energy-elastic state. Considering unfilled elastomers they are small also in the entropy-elastic state. Indeed, with filled elastomers the dissipative effects become significant. In order to extract the information concerning the molecular interpretation of the loss factor, these dissipative effects must be separated. A visual sign for the dissipative part is the baseline offset between the start and the end point of the loss factor distribution, see Fig. 2 and 3. The separation of the dissipative part can be done geometrically by applying a suitable iterative baseline correction function (BLC) of the form shown in Eq.(6), using a transient function $\alpha(T)$, Eq.(9), which is a normalised cumulative partition variable, in order to adjust the baseline weights along the loss factor curve. This baseline function regards that on both sides normally the loss factor curve ends in plateau values. The given form of the BL shown in Eq.(6) allows to consider small non-plateau situations including the slopes S_A and S_B at T_A and T_B. Clearly to say, it is always better to measure the loss factor in a sufficient temperature range in order to approximate the plateau values on both sides. However, there can be difficult situations in that on the high temperature side a minimum in loss factor appears. Then consistent evaluations are necessary in ageing investigations or in considering deformation frequency dependence. With the evaluations presented here the slope terms have been set to zero in using Eq.(8).

$$BL_\alpha(T) = (1-\alpha(T))\cdot\left[\tan\delta(T_A) + S_A\cdot T_{st}\right] + \alpha(T)\cdot\left[\tan\delta(T_B) + S_B\cdot(1-T_{st})\right] \tag{6}$$

$$T_{st} = \frac{T - T_A}{T_B - T_A} \tag{7}$$

$$BL_\alpha(T) = (1-\alpha(T))\cdot\tan\delta(T_A) + \alpha(T)\cdot\tan\delta(T_B) \tag{8}$$

$$\alpha(T) = \frac{\int_{T_A}^{T}\tan\delta(T)dT}{\int_{T_A}^{T_B}\tan\delta(T)dT} \tag{9}$$

$$D_k = \sum_{T_A}^{T_B} (\tan\delta\_I_{k-1}(T_i) - \tan\delta\_I_k(T_i))^2 \qquad (10)$$

$BL_\alpha(T)$ baseline correction function based on $\alpha(T)$ between T_A and T_B;
$\alpha(T)$ normalised cumulative partition function of $\tan\delta(T)$, in [-];
T_A lower baseline setting temperature with slope S_A, in [°C];
T_B upper baseline setting temperature with slope S_B, in [°C];
T_{st} scaled temperature, in [°C];
S_A slope at T_a in $\tan\delta(T_A)$, in [1/°C];
S_B slope at T_b in $\tan\delta(T_B)$, in [1/°C];
T measurement temperature between T_A and T_B, in [°C];
$\tan\delta(T_A)$ value of uncorrected $\tan\delta(T)$ at temperature T_A, in [-];
$\tan\delta(T_B)$ value of uncorrected $\tan\delta(T)$ at temperature T_B, in [-];
D_k assessment parameter for the k^{th} iteration cycle, k = 1, 2, 3, …;
$\tan\delta\_I_k\text{-}1(T_i)$ value of loss factor at temperature T_i in $(k\text{-}1)^{th}$ iteration cycle;
$\tan\delta\_I_k(T_i)$ value of loss factor at temperature T_i in $(k)^{th}$ iteration cycle.

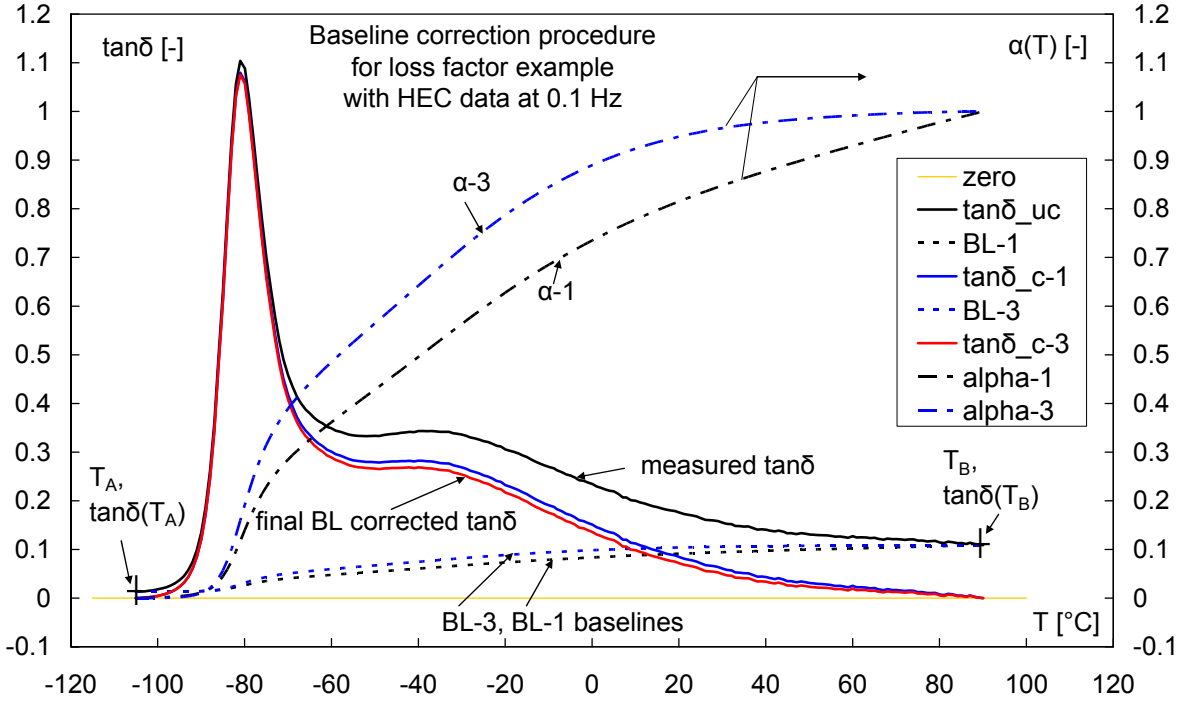

Figure 7: Example of a baseline correction procedure of the loss factor of HEC HX1. Shown are the iteration steps 1 and 3. After 3 iterations the calculations already reached convergence.

In the following, the iterative procedure used to find the final baseline is outlined.

Iteration cycle k = 1

(1.1) Calculation of $\alpha(T)$ from the uncorrected curve, $\tan\delta\_I_0(T_i)$. (1.2) Establishing the BL according to Eq.(6) or Eq.(8). (1.3) First BL correction of the uncorrected curve, formation of $\tan\delta\_I_1(T_i)$. (1.4) Calculation of the assessment parameter D_1.

Iteration cycle k = 2

(2.1) Calculation of $\alpha(T)$ from the first corrected curve, $\tan\delta\_I_1(T_i)$. (2.2) Establishing the BL. (2.3) Second BL correction of the **un**corrected curve, formation of $\tan\delta\_I_2(T_i)$. (2.4) Calculation of the assessment parameter D_2.

Iteration cycle k = n

(n.1) Calculation of $\alpha(T)$ from the n-1 corrected curve, $\tan\delta\_I_{n-1}(T_i)$. (n.2) Establishing the BL. (n.3) nth BL correction of the **un**corrected curve, formation of $\tan\delta\_I_n(T_i)$. (n.4) Calculation of the assessment parameter D_n.

During iteration the value of D_k defined in Eq.(10) becomes smaller. The iteration is stopped after D_k falls below $D_{k\text{-limit}}$. Mostly 0.01 to 0.001 are good choices for $D_{k\text{-limit}}$. Fig. 10 illustrates the BLC procedure for HEC HX1. The iteration procedure is fast and stable. Usually after 3 to 6 cycles the final baseline corrected curve has been reached. In Fig. 7 also the course of the $\alpha(T)$ can be seen. Fig. 8 and 9 show examples of baseline corrected loss factor curves of HEC HX1 and of an ageing series of CRP1.

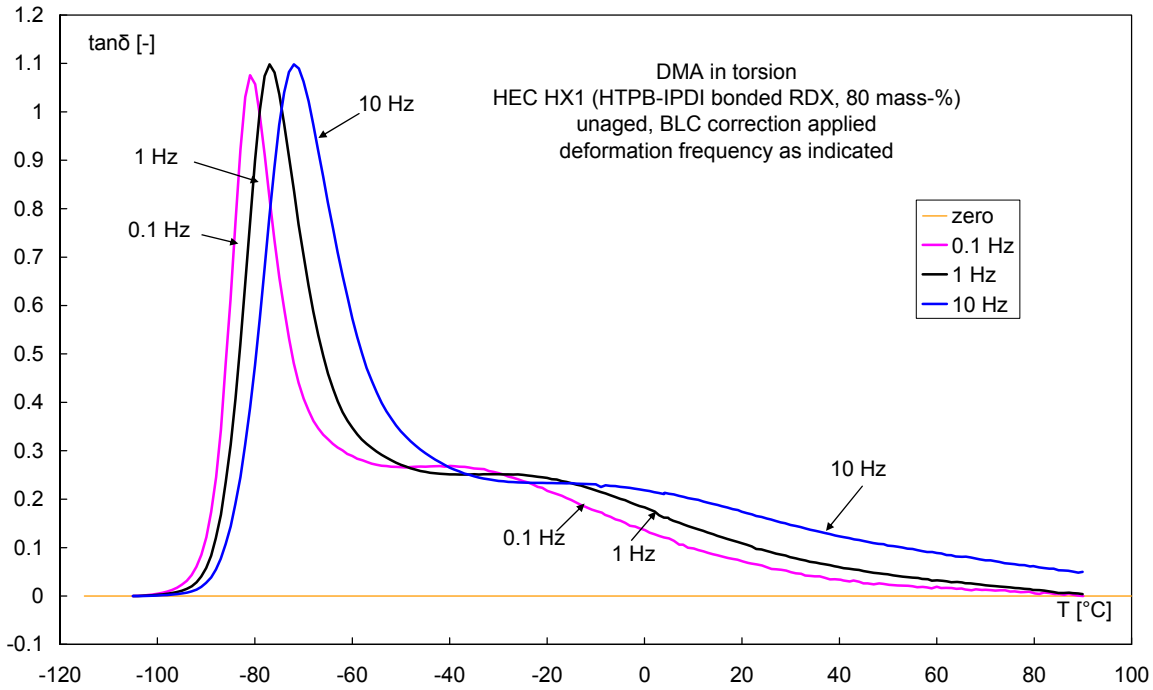

Figure 8: Baseline corrected loss factor curves of the HEC HX1 at three different deformation frequencies. See Fig. 2 for the original curves.

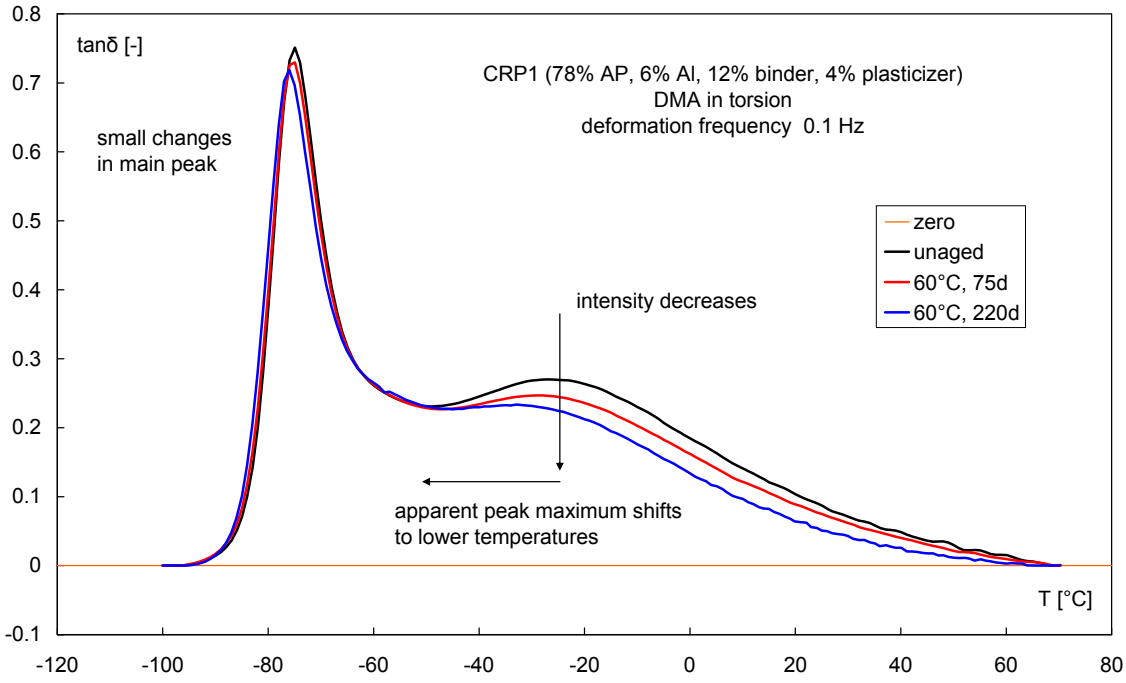

Figure 9: Baseline corrected loss factor curves at different ageing times of CRP1. Ageing temperature was 60°C. For interpretation see [1, 3, 4, 5].

3.2 Modelling of the loss factor curve

After the baseline correction procedure a suitable fit function must be chosen in order to evaluate the areas under the peaks of the loss factor curve. The function must describe the experimental data and extract from them the indications for the different regions of molecular rearrangement processes. If the values of the interaction energies and the molecular docking regions are randomly distributed in the isotropic material, a Gauss distribution, Eq.(11) should describe the processes. But, as clearly visible in Fig. 8 and 9, the shapes of the loss factor curves are not symmetrical as a Gauss distribution, meaning that some dissipative parts still remain in the experimental data. These dissipative effects can be described with relaxation curves, which mostly can be represented with exponentially decreasing functions, see Eq.(12). The combined processes are described by an exponentially modified Gauss (EMG) distribution function, shown in Eq.(13), which is mathematically a convolution between Eq.(11) and Eq.(12). In Eq.(14) a sum of EMGs is given, because the whole loss factor curve is composed of several transition processes. The application of EMG function to model loss factor function was first reported in [11].

$$f_G(T) = \frac{A}{w \cdot \sqrt{2\pi}} \cdot \exp\left[-0.5 \cdot \left(\frac{T - Tc}{w} \right)^2 \right] \tag{11}$$

$$f_E(T) = \exp\left(-\frac{T}{To} \right) \tag{12}$$

$$f_{EMG}(T) = \frac{A}{To} \cdot \frac{1}{2} \cdot \exp\left[0.5 \cdot \left(\frac{w}{To} \right)^2 - \frac{T - Tc}{To} \right] \cdot \left\{ 1 - \mathrm{erf}\left[-\frac{1}{\sqrt{2}} \cdot \left(\frac{T - Tc}{w} - \frac{w}{To} \right) \right] \right\} \tag{13}$$

$$\tan\delta_{BLC} = td_0 + \sum_{i=1}^{N} \frac{A_i}{To_i} \cdot \frac{1}{2} \exp\left[0.5 \left(\frac{w_i}{To_i} \right)^2 - \frac{T - Tc_i}{To_i} \right] \left\{ 1 - \mathrm{erf}\left[-\frac{1}{\sqrt{2}} \left(\frac{T - Tc_i}{w_i} - \frac{w_i}{To_i} \right) \right] \right\} \tag{14}$$

T measurement temperature, in [°C];
$\tan\delta_{BLC}$ value of the loss factor as function of T after the BLC, in [-];
A_i peak areas of the EMG peaks, also equal to the areas of the corresponding Gauss peaks alone, in [°C];
w_i half peak width at half height of only the Gaussian part, in [°C];
Tc_i temperature at peak maxima in the Gaussian part of the EMG (not the peak maxima of EMG), in [°C];
To_i relaxation parameter in exponential part of EMG, also named as τ, in [°C];
td_0 to consider an eventually residual offset in $\tan\delta$ data, in [-];
N number of EMG fit functions;
erf error function; erf(x) = -erf(-x).

Note that the peak area A has here the formal dimension of the temperature unit used of the abscissa: [$\tan\delta$]*[T] = [°C]. With a value of N equal to the extractable mobility ranges Eq.(14) is adjusted to the baseline corrected experimental data by non-linear fit algorithms. Here a Levenberg-Marquardt algorithm was used provided by the programme package Origin™ [12].

In Fig. 10 the modelling of the loss factor of HEC HX1 at 0.1 Hz deformation frequency is presented. The description of the data is very good, with high correlation coefficient. In comparison, Fig. 11 shows the modelling with pure Gauss functions. The description is only approximate but qualitatively usable. It can help to identify some positions of the first two peaks named P1 and P2 for the EMG fits. It is obvious now that the residual dissipative effect must be regarded in the description.

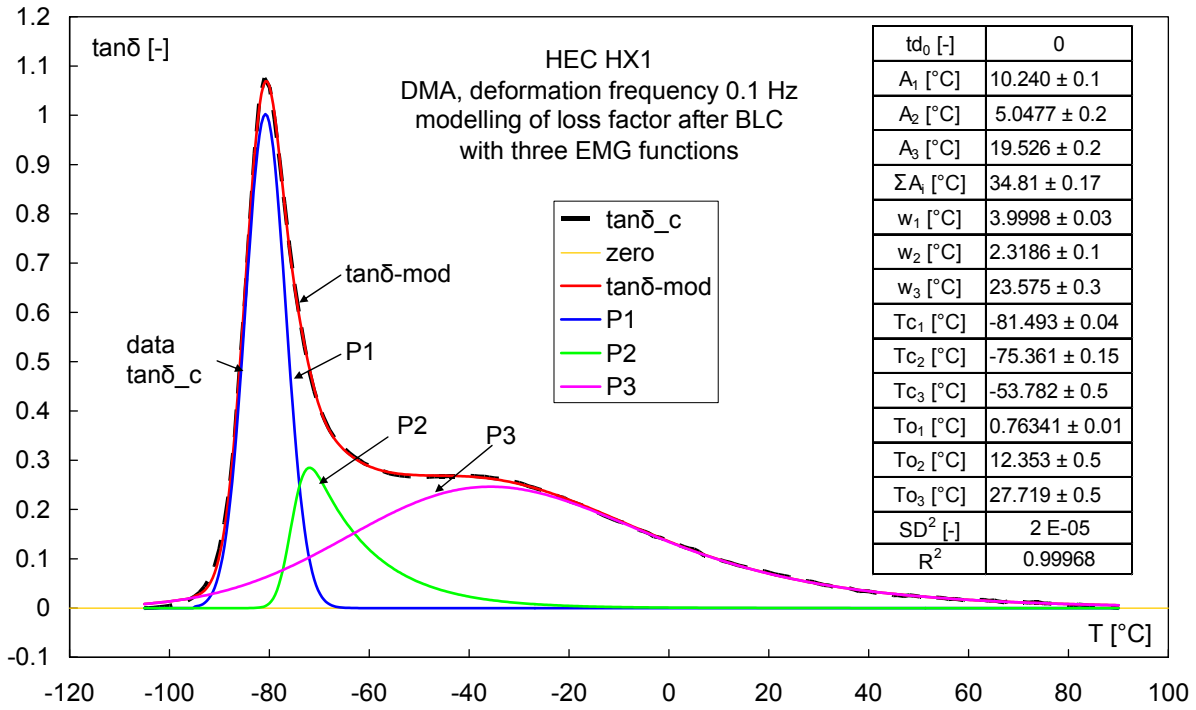

Figure 10: Modelling of tanδ with three EMG functions. The description is very good with a high correlation coefficient.

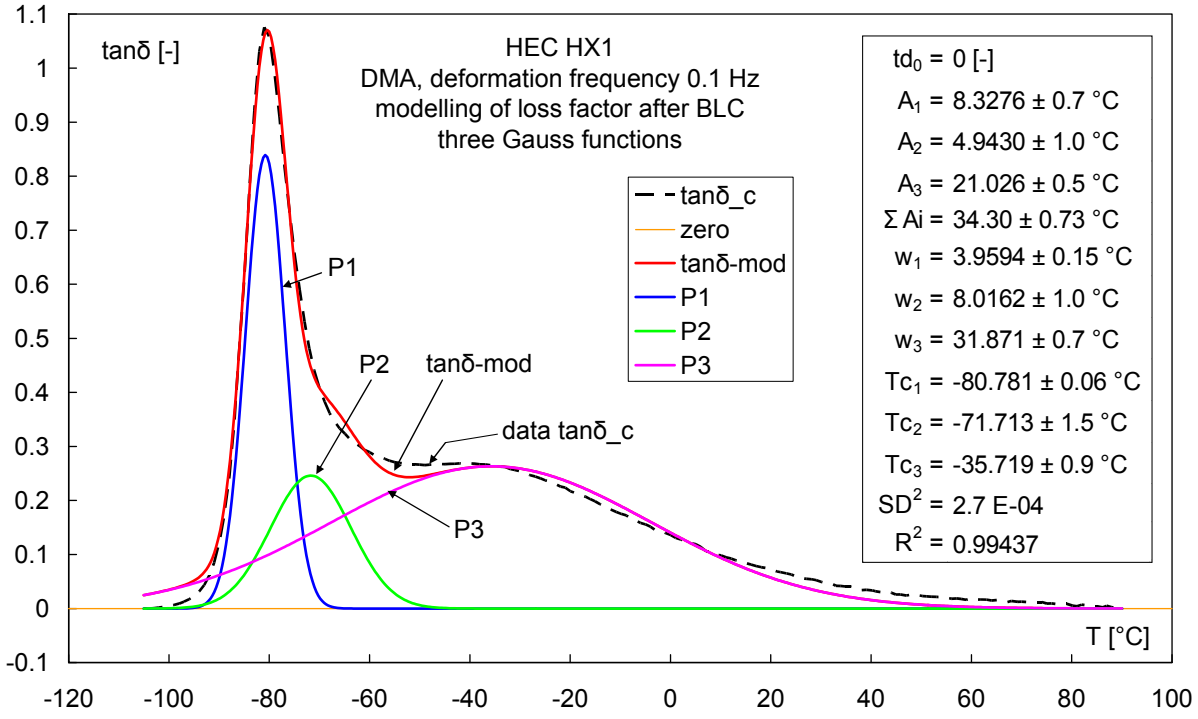

Figure 11: Modelling of loss factor of HEC HX1 with three Gauss distributions. The description is only approximate.

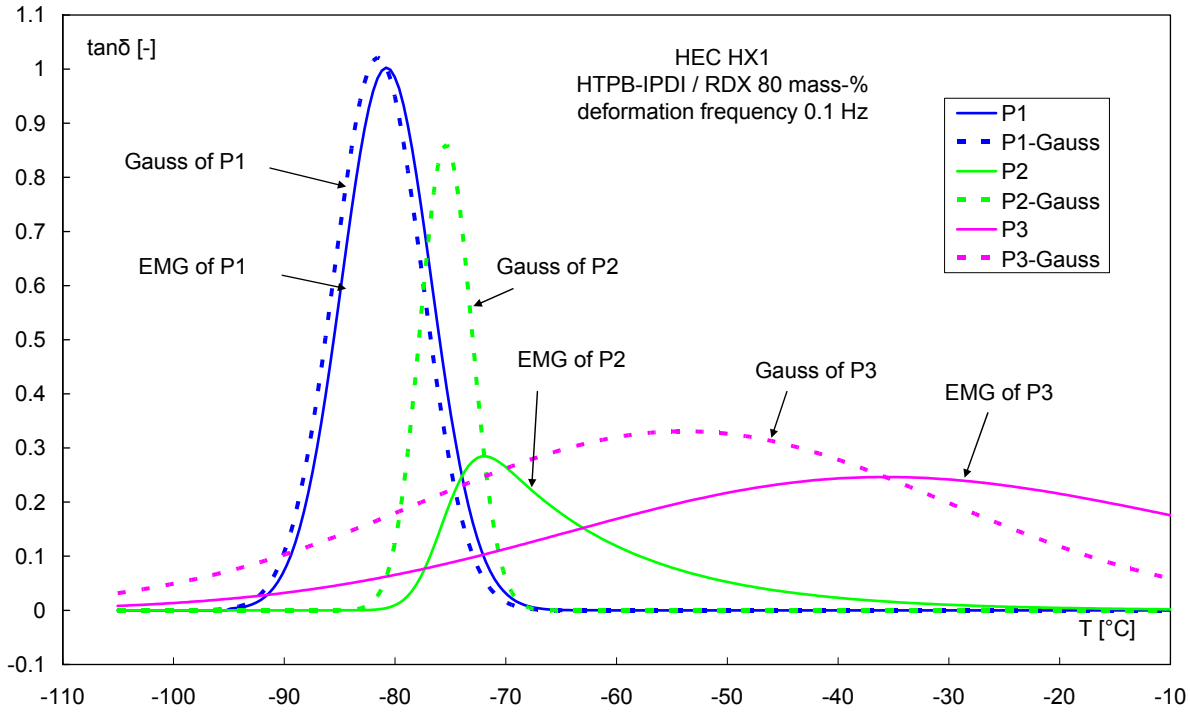

Figure 12: Representation of the formal Gauss peak and EMG peak of the three transitions. The maximum of every EMG curves lies on the corresponding Gauss function.

Fig. 12 shows an example of the EMG peaks together with their corresponding Gaussian parts. The maxima of the EMG peaks lie always on the corresponding Gaussian curves. Depending on the relative weight of the dissipative part, the EMG functions are moving from the maximum of the Gauss curves to the base, meaning from non-dissipative to totally dissipative behaviour. The exponential parts of the EMGs in the example of Fig. 12 can be seen in Fig. 13.

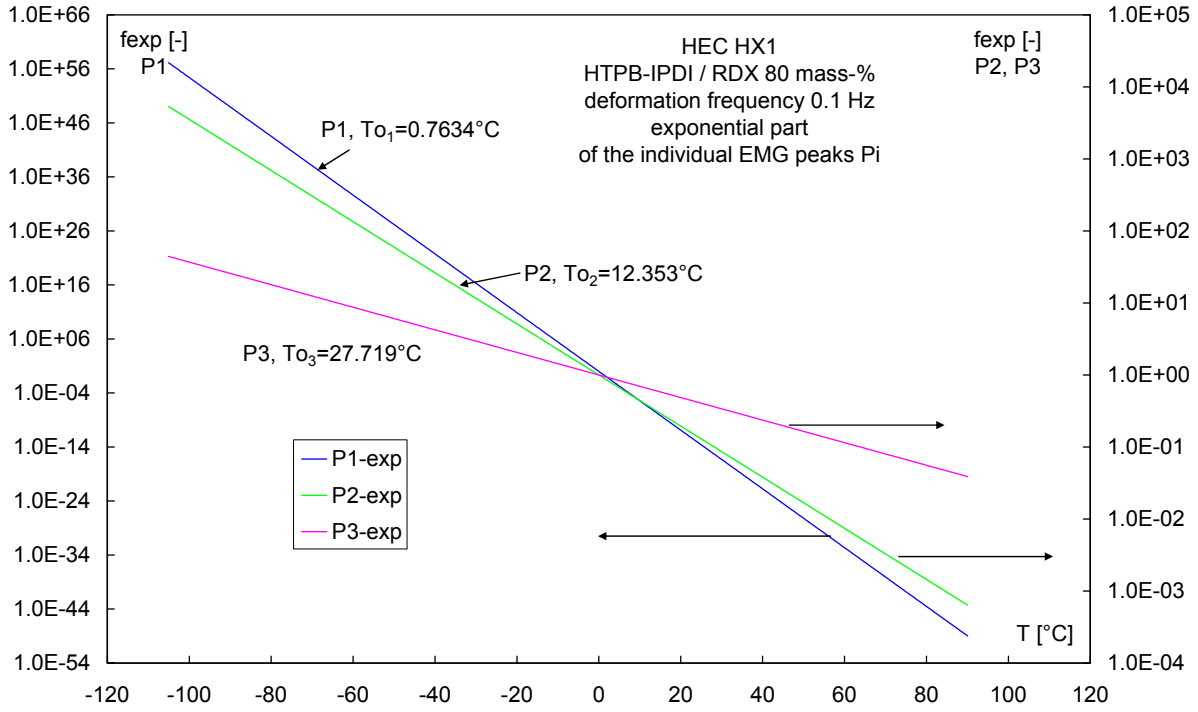

Figure 13: Exponential parts of the EMGs of the example used in Fig. 12.

A note to the number of fit parameters should be given. The number of fit parameters is equal to N*4, whereby N is the number of EMGs and 4 is the number of parameters per EMG: A_i, w_i, Tc_i, To_i. Considering N=3 EMGs one has to find 12 parameters in a unique way. This is possible due to the inbuilt limitations of the EMG function in reproducing the shape of functions or curves. This means the EMG contains the constraints within its mathematical structure and cannot describe any shape. However, one must have the necessary shape structure in the loss factor data to determine the parameters uniquely. The following examples shown in Table 9 illustrate this aspect. All are based on the data of HEC HX1 at 0.1 Hz deformation frequency. In Table 9 four sets of parameter determinations are compared. The parameters of fits 1 to 3 are all within the standard deviation for each fit. The initial parameter settings have been varied by about 2% to 3%. With fit 4 this variation was about 10% from the values of fit 1 to 3. The search procedure has found another solution, which has even a slightly higher correlation coefficient. These data are compared in Fig.14. The main variation is with peak 1 and peak 2, whereby peak 3 stays quite similar in both fit situations. The explanation is that two peaks are definitely given in the structure of the curve. The third peak is more or less 'hidden', which means for its presence the total curve gives no unique part in its shape. This gives some freedom to the fit algorithm for choosing the values in size, shape and position.

Table 9: Comparison of fits and their parameters obtained with HEC HX1 at 0.1 Hz deformation frequency. R^2: correlation coefficient; SD: standard deviation. The lower part of this Table shows the parts of each sub-transition with regard to the total transition. The three sub transitions reflect three binder fractions with different molecular mobility.

quantity	**Fit 1**	**Fit 2**	**Fit 3**	**SD**	**Fit 4**	**SD**
td_0 [-]	0	0	0	-	0	-
A_1 [°C]	10.240	10.245	10.157	0.1	5.8616	0.3
A_2 [°C]	5.0477	5.0628	5.0591	0.2	10.431	0.2
A_3 [°C]	19.526	19.480	19.575	0.2	18.478	0.2
$\sum A_i$ [°C]	34.814	34.788	34.791	0.17	34.77	0.23
w_1 [°C]	3.9998	4.0035	3.9767	0.03	4.1924	0.08
w_2 [°C]	2.3186	2.3027	2.3658	0.1	2.2467	0.05
w_3 [°C]	23.575	23.545	23.564	0.3	22.084	0.3
Tc_1 [°C]	-81.493	-81.488	-81.522	0.06	-83.959	0.15
Tc_2 [°C]	-75.361	-75.35	-75.485	0.15	-83.54	0.05
Tc_3 [°C]	-53.782	-53.727	-53.917	0.5	-52.126	0.4
To_1 [°C]	0.76341	0.76231	0.76321	0.03	2.3713	0.3
To_2 [°C]	12.353	12.427	12.152	0.5	13.586	0.5
To_3 [°C]	27.719	27.721	27.758	0.5	28.483	0.3
SD^2 of fit [-]	2 E-05	2 E-05	2 E-05	-	6.2E-06	-
R^2 of fit [-]	0.99968	0.99967	0.99967	-	0.99987	-

Percentages of binder fraction areas from the total transition region area						
	Fit 1		**Fit 2**		**Fit 3**	
	[°C]	**%**	**[°C]**	**%**	**[°C]**	**%**
A_1 [°C]	10.240	29.4	10.245	29.4	10.157	29.2
A_2 [°C]	5.0477	14.5	5.0628	14.6	5.0591	14.5
A_3 [°C]	19.526	56.1	19.480	56.0	19.575	56.3
$\sum A_i$ [°C]	34.814	100.0	34.788	100.0	34.791	100.0

In principle both solutions are correct, if one has no additional information or knowledge about the probable structure of the third peak, here named P2. Such problems can also arise with not well defined experimental data means in the presence of noise and scattering. Then it becomes even useless to try a description with three peaks, even if three processes are really happening. The way out is to use less peaks in the description. The present loss factor curve is structured in such a way to support clearly and even uniquely the parameter fit with two peaks. The result is shown in Fig. 15. The peak 3 is nearly the same in both determinations. Peak 1 from two EMGs comprises the peak 1 together with peak 2 from three EMGs. Only a part of peak 2 from 3 EMGs is represented by peak 2 from 2 EMGs, which corresponds to peak 3 from 3 EMGs. In this way the two main structural features of the loss factor curve are described and an evaluation of experimental data obtained with an impact variation such as deformation frequency or ageing is easily possible.

The lower part of Table 9 shows a sub-table with interesting data. The three transition regions of the binder found by EMG modelling have different weights with regard to the total transition region. The percentages of the three areas of the sub-transitions with respect to the total transition area are given. Clearly to say, most of the binder fraction is mobility hindered or restricted. The large part evidently identified as ‘second peak’ (here named third peak) comprises alone more than half of the binder. Together with the second peak obtained by modelling more than two third of the binder is mobility restricted, because only peak 1 is assigned to the unrestricted binder.

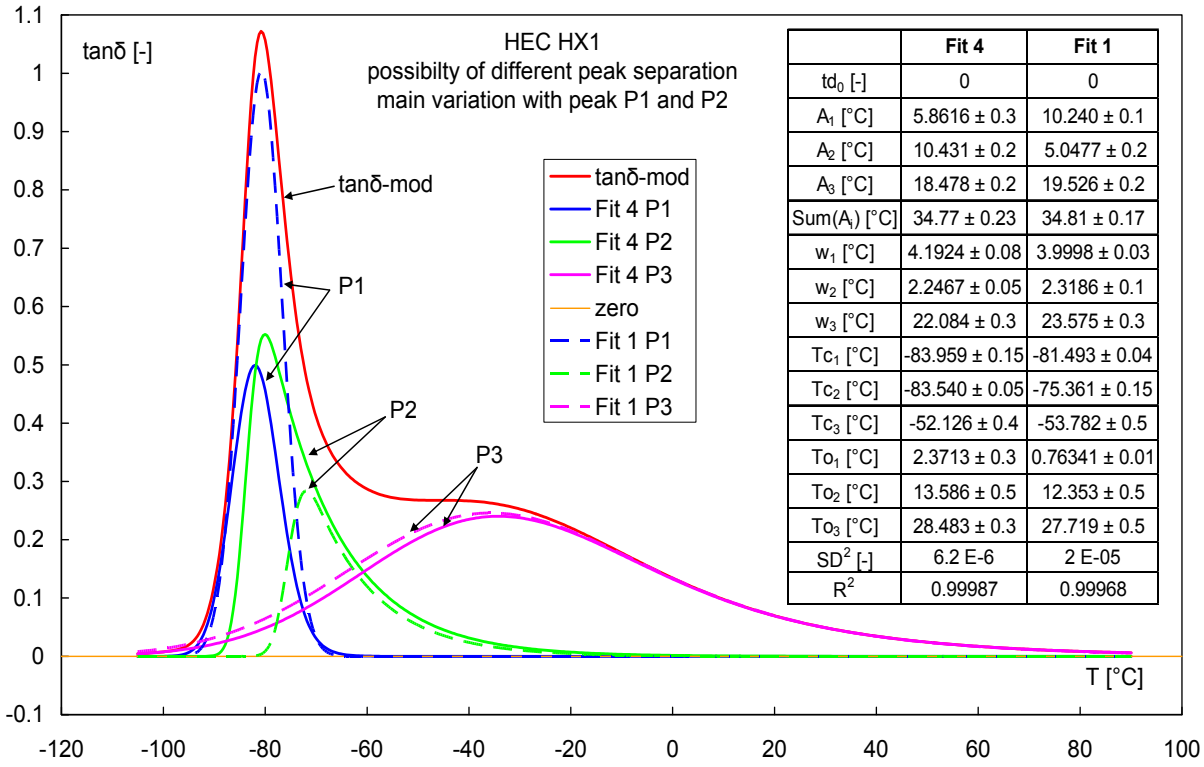

	Fit 4	Fit 1
td_0 [-]	0	0
A_1 [°C]	5.8616 ± 0.3	10.240 ± 0.1
A_2 [°C]	10.431 ± 0.2	5.0477 ± 0.2
A_3 [°C]	18.478 ± 0.2	19.526 ± 0.2
Sum(A_i) [°C]	34.77 ± 0.23	34.81 ± 0.17
w_1 [°C]	4.1924 ± 0.08	3.9998 ± 0.03
w_2 [°C]	2.2467 ± 0.05	2.3186 ± 0.1
w_3 [°C]	22.084 ± 0.3	23.575 ± 0.3
Tc_1 [°C]	-83.959 ± 0.15	-81.493 ± 0.04
Tc_2 [°C]	-83.540 ± 0.05	-75.361 ± 0.15
Tc_3 [°C]	-52.126 ± 0.4	-53.782 ± 0.5
To_1 [°C]	2.3713 ± 0.3	0.76341 ± 0.01
To_2 [°C]	13.586 ± 0.5	12.353 ± 0.5
To_3 [°C]	28.483 ± 0.3	27.719 ± 0.5
SD^2 [-]	6.2 E-6	2 E-05
R^2	0.99987	0.99968

Figure 14: Comparison of two descriptions with three EMGs at 0.1 Hz. The main difference is found with peak 1 and peak 2.

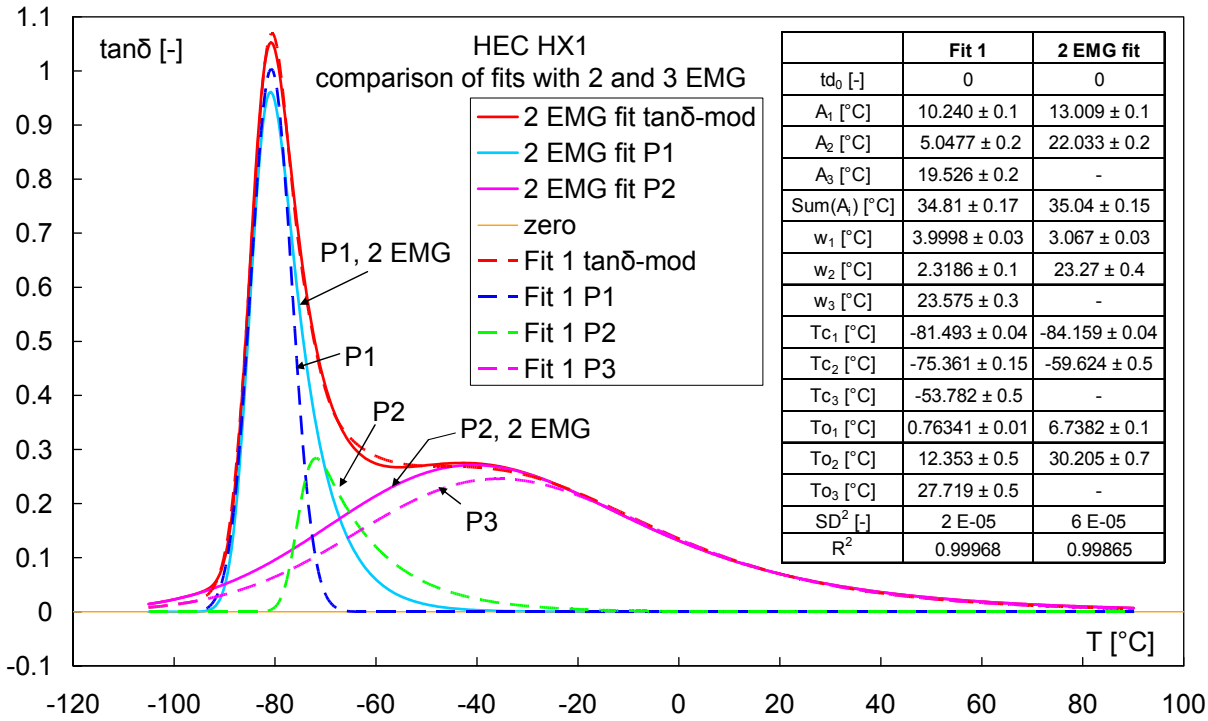

	Fit 1	2 EMG fit
td_0 [-]	0	0
A_1 [°C]	10.240 ± 0.1	13.009 ± 0.1
A_2 [°C]	5.0477 ± 0.2	22.033 ± 0.2
A_3 [°C]	19.526 ± 0.2	-
Sum(A_i) [°C]	34.81 ± 0.17	35.04 ± 0.15
w_1 [°C]	3.9998 ± 0.03	3.067 ± 0.03
w_2 [°C]	2.3186 ± 0.1	23.27 ± 0.4
w_3 [°C]	23.575 ± 0.3	-
Tc_1 [°C]	-81.493 ± 0.04	-84.159 ± 0.04
Tc_2 [°C]	-75.361 ± 0.15	-59.624 ± 0.5
Tc_3 [°C]	-53.782 ± 0.5	-
To_1 [°C]	0.76341 ± 0.01	6.7382 ± 0.1
To_2 [°C]	12.353 ± 0.5	30.205 ± 0.7
To_3 [°C]	27.719 ± 0.5	-
SD^2 [-]	2 E-05	6 E-05
R^2	0.99968	0.99865

Figure 15: Comparison of two descriptions: one with three EMGs, the other with two EMGs at 0.1 Hz. The main difference arises in the range of the main peak.

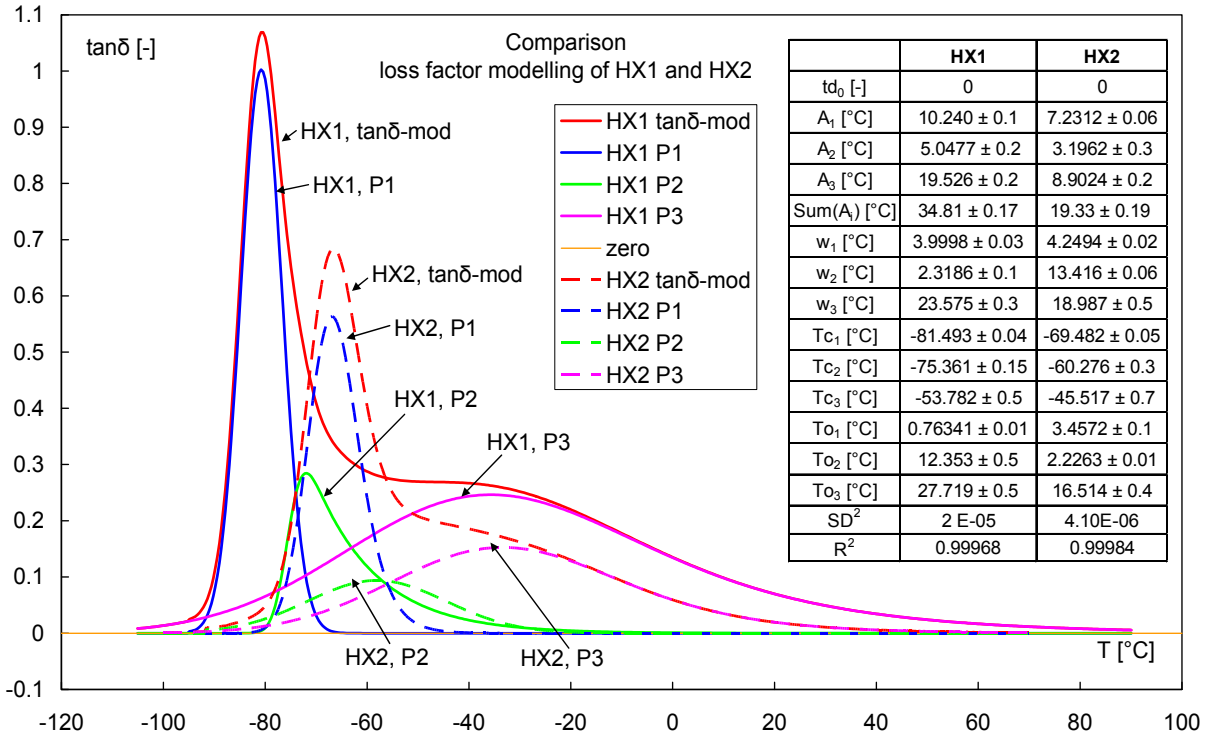

	HX1	HX2
td_0 [-]	0	0
A_1 [°C]	10.240 ± 0.1	7.2312 ± 0.06
A_2 [°C]	5.0477 ± 0.2	3.1962 ± 0.3
A_3 [°C]	19.526 ± 0.2	8.9024 ± 0.2
Sum(A_i) [°C]	34.81 ± 0.17	19.33 ± 0.19
w_1 [°C]	3.9998 ± 0.03	4.2494 ± 0.02
w_2 [°C]	2.3186 ± 0.1	13.416 ± 0.06
w_3 [°C]	23.575 ± 0.3	18.987 ± 0.5
Tc_1 [°C]	-81.493 ± 0.04	-69.482 ± 0.05
Tc_2 [°C]	-75.361 ± 0.15	-60.276 ± 0.3
Tc_3 [°C]	-53.782 ± 0.5	-45.517 ± 0.7
To_1 [°C]	0.76341 ± 0.01	3.4572 ± 0.1
To_2 [°C]	12.353 ± 0.5	2.2263 ± 0.01
To_3 [°C]	27.719 ± 0.5	16.514 ± 0.4
SD^2	2 E-05	4.10E-06
R^2	0.99968	0.99984

Figure 16: Comparison of the loss factor modelling with three EMGs of HX1 and HX2 at 0.1 Hz.

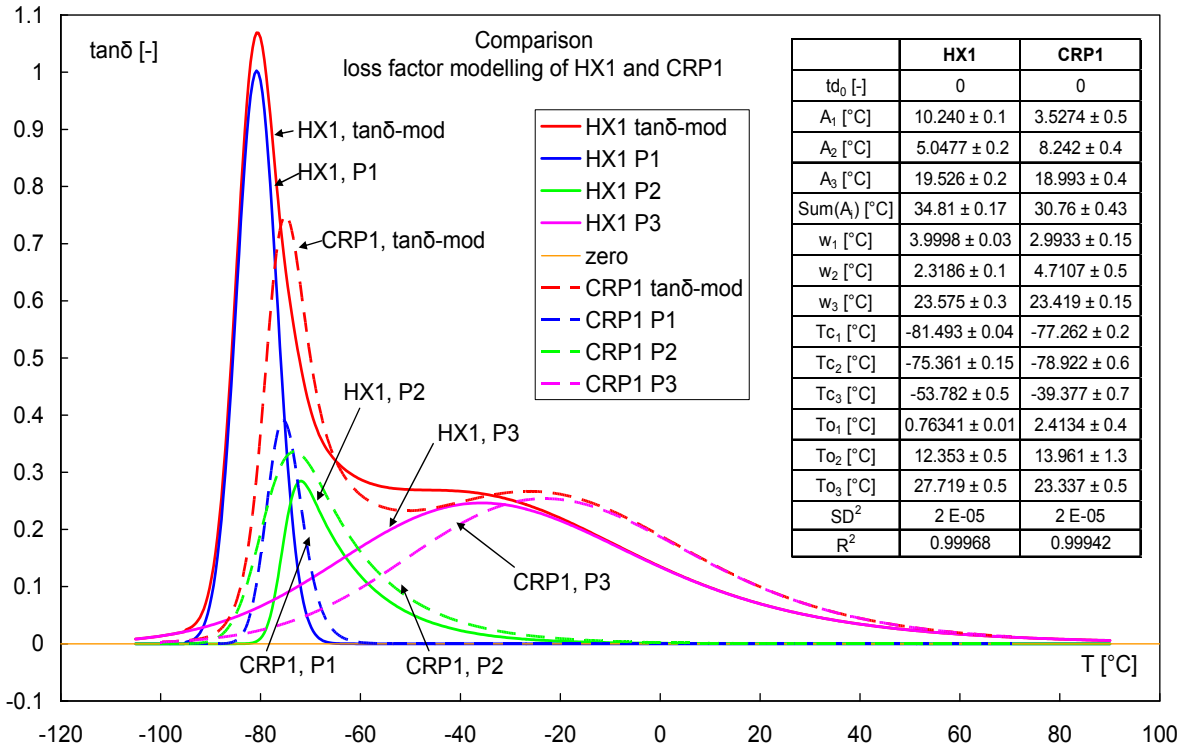

	HX1	CRP1
td_0 [-]	0	0
A_1 [°C]	10.240 ± 0.1	3.5274 ± 0.5
A_2 [°C]	5.0477 ± 0.2	8.242 ± 0.4
A_3 [°C]	19.526 ± 0.2	18.993 ± 0.4
Sum(A_i) [°C]	34.81 ± 0.17	30.76 ± 0.43
w_1 [°C]	3.9998 ± 0.03	2.9933 ± 0.15
w_2 [°C]	2.3186 ± 0.1	4.7107 ± 0.5
w_3 [°C]	23.575 ± 0.3	23.419 ± 0.15
Tc_1 [°C]	-81.493 ± 0.04	-77.262 ± 0.2
Tc_2 [°C]	-75.361 ± 0.15	-78.922 ± 0.6
Tc_3 [°C]	-53.782 ± 0.5	-39.377 ± 0.7
To_1 [°C]	0.76341 ± 0.01	2.4134 ± 0.4
To_2 [°C]	12.353 ± 0.5	13.961 ± 1.3
To_3 [°C]	27.719 ± 0.5	23.337 ± 0.5
SD^2	2 E-05	2 E-05
R^2	0.99968	0.99942

Figure 17: Comparison of the loss factor modelling with three EMGs of HX1 and CRP1 at 0.1 Hz.

In Fig. 16 the EMG description of HEC HX1 and HEC HX2, here named HX1 and HX2, is compared. The total loss factor intensity of HX2 is only about half of the intensity of HX1. The position of the first maximum is at significantly higher temperature. The reason is the lower plasticiser content, 1 mass-% against 8 mass-%. Moreover , the use of HTPB R45HT as prepolymer results in a higher cross-linking density, which reduces the mobility of the binder chains.

The temperature corresponding to the EMG maximum of the second apparent transition of HX2 has nearly the same value as the one of HX1. This information could not be obtained from the total loss factor curves alone by determining the maximum temperatures directly. Only by the modelling this is recognisable. A further interesting comparison is made in Fig. 17 between HX1 and CRP1. The total intensities, the sums over the Ai, of the two loss factors are similar, namely 34.8 and 31.0, but the transition contributions to them are different. With HX1 the two lower temperature transitions contribute about 44 % and with CRP1 this is only 38 %. The second apparent peak of CRP1 is more intense and positioned at higher temperatures. The reason is the binder shell around the AP particles created by the reactive bonding agent used, which forms an elastomer network with higher glass-rubber transition temperature and thereby the transition intensity of this region is increased.

4 Quantification of changes in loss factor curves by experimental impacts

4.1 Modelling of the loss factor curve changed by deformation frequency sweep

In this section the effect on the loss factor by changing the deformation frequency is modelled. The Figs 21, 22 and 23 show the modelling of the loss factor of HX1 at 1 Hz, 10 Hz and 30 Hz deformation frequencies. The modelling of the curve determined at 0.1 Hz was already shown above. The curves change systematically, which can be seen in the overview given in Fig. 24. The maximum temperatures named Tc_i shift to higher temperature values, the individual intensities A_i increase, the peak widths w_i increase and the relaxation parameters To_i increase. The quantitative data are given in Table 10.

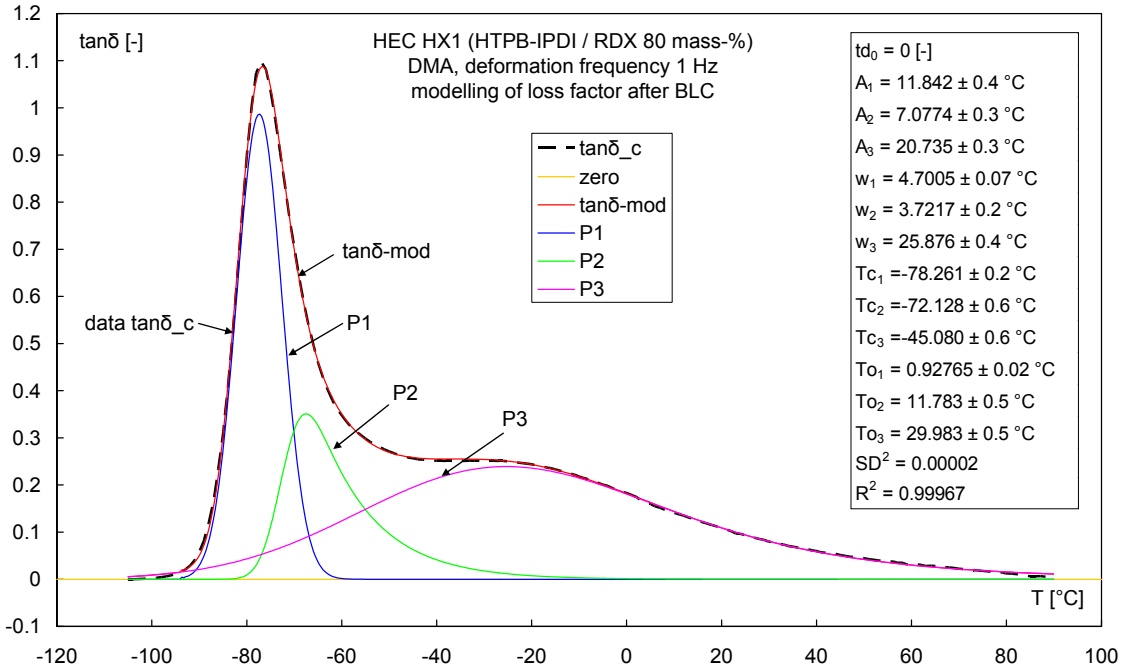

Figure 18: Description of the loss factor of the unaged HEC HX1 with three EMG functions at 1 Hz deformation frequency.

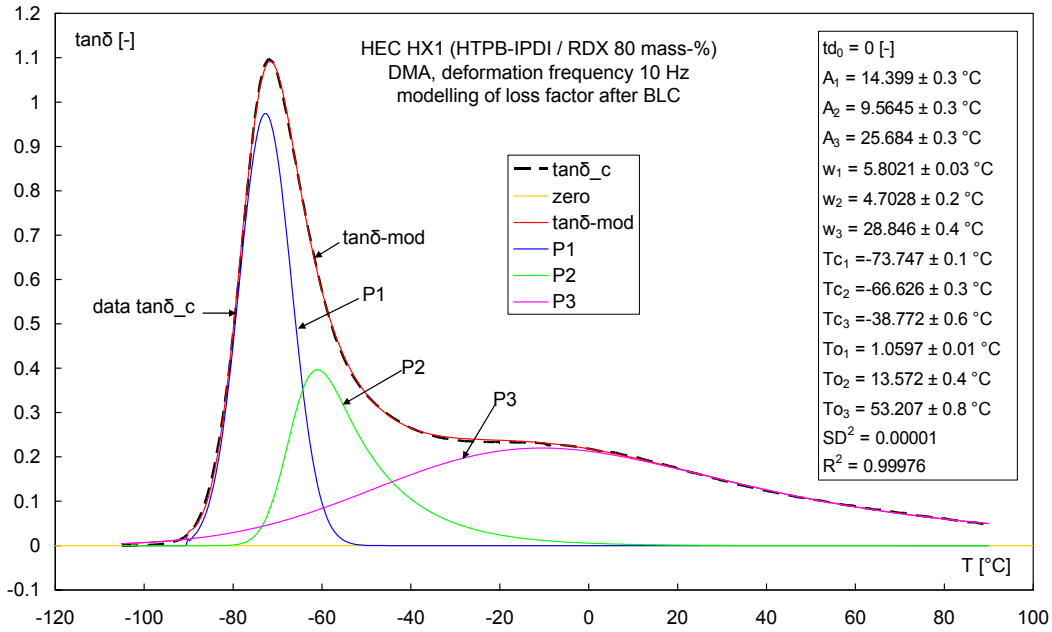

Figure 19: Description of the loss factor of the unaged HEC HX1 with three EMG functions at 10 Hz deformation frequency.

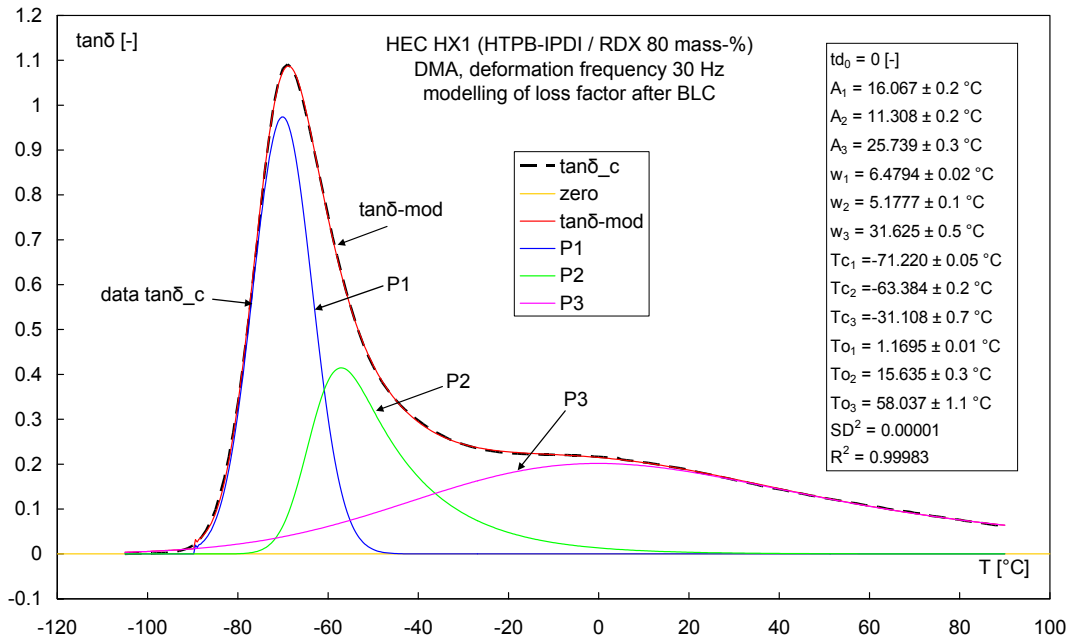

Figure 20: Description of the loss factor of the unaged HEC HX1 with three EMG functions at 30 Hz deformation frequency.

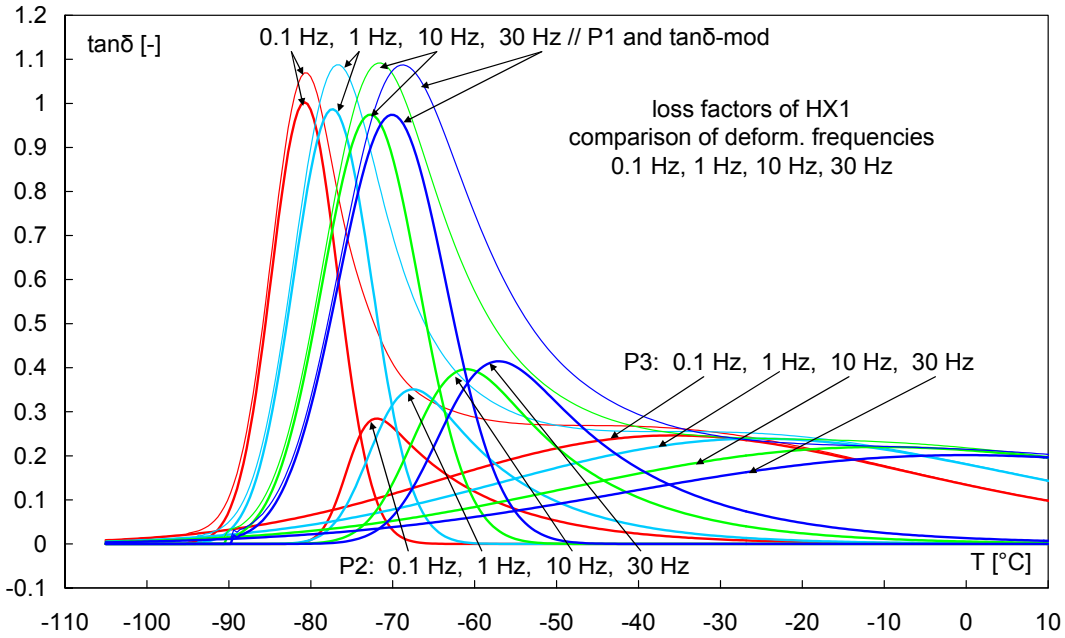

Figure 21: Overview of the description of the loss factor of the unaged HEC HX1 with three EMG functions at four deformation frequencies.

Some of the changes by going from 0.1 Hz to 30 Hz are highlighted. The peak 2 shows major changes in A_2 and w_2, whereas peak 3 shows the greatest changes in Tc_3 and To_3. The increase in the relaxational part (To_i) indicates the increasing of dissipative effects, mainly by 'molecular friction'. The strong increase in maximum temperature with deformation rate indicates the possibility of high energy dissipation and therefore a heating up of the material already at moderate low temperature. This effect has particular and severe implications for rocket motor propellants: it is dominant in the mobility range of the hindered binder, expressed in peak 3. Peak 2 is seen to represent the restricted binder by the filler particles, here RDX. The peak 1 gives the behaviour of the unrestricted binder. With regard to the general peak broadening by increasing deformation rate, the peak 1 stays constant in intensity. Considering the total behaviour, it becomes clear that the essential information about

the influence of a parameter or impact change is contained in peak 2 and peak 3. Peak 1 contains no information about such an influence. This was also found with the ageing of composite rocket propellant formulations based on HTPB-IPDI, see [1, 2, 5]. In part the content of this section was presented already in [13]. In Table 11 the description of the changes in the EMG parameters as function of deformation frequency is compiled.

Table 10: EMG parameters of the description of loss factor curves of HEC HX1 at several deformation frequencies. FP_i: fit parameter; R^2: correlation coefficient; SD: standard deviation.

FP_i	**0.1 Hz**	**1.0 Hz**	**10 Hz**	**30 Hz**	**ratio FP_i(at 30 Hz) to FP_i(at 0.1 Hz)**
td_0 [-]	0	0	0	0	0
A_1 [°C]	10.24 ± 0.1	11.84 ± 0.4	14.40 ± 0.3	16.07 ± 0.2	1.57
A_2 [°C]	5.048 ± 0.2	7.077 ± 0.3	9.565 ± 0.3	11.31 ± 0.2	**2.24**
A_3 [°C]	19.53 ± 0.2	20.74 ± 0.3	25.68 ± 0.3	25.74 ± 0.3	1.32
$\sum A_i$ [°C]	34.81 ± 0.17	39.65 ± 0.33	49.65 ± 0.3	53.11± 0.23	-
w_1 [°C]	4.00 ± 0.03	4.701 ± 0.07	5.802 ± 0.03	6.479 ± 0.02	1.62
w_2 [°C]	2.32 ± 0.1	3.723 ± 0.2	4.703 ± 0.2	5.178 ± 0.1	**2.23**
w_3 [°C]	23.58 ± 0.3	25.88 ± 0.4	28.85 ± 0.4	31.63 ± 0.5	1.34
Tc_1 [°C]	-81.49 ±0.04	-78.26 ± 0.2	-73.75 ± 0.1	-71.22 ±0.05	10.3
Tc_2 [°C]	-75.36 ±0.15	-72.13 ± 0.6	-66.63 ± 0.3	-63.38 ± 0.2	12
Tc_3 [°C]	-53.78 ± 0.5	-45.08 ± 0.6	-38.77 ± 0.6	-31.11 ± 0.7	**22.7**
To_1 [°C]	0.763 ±0.01	0.928 ±0.02	1.060 ± 0.01	1.170 ± 0.01	1.53
To_2 [°C]	12.35 ± 0.5	11.78 ± 0.5	13.57 ± 0.4	15.64 ± 0.3	1.27
To_3 [°C]	27.72 ± 0.5	29.98 ± 0.5	53.21 ± 0.8	58.04 ± 1.1	**2.09**
SD^2 of fit [-]	2 E-05	2 E-05	1 E-05	1 E-05	-
R^2 of fit	0.99968	0.99967	0.99976	0.99983	-

Table 11: Description of the fit parameters of the EMGs of loss factors of HEC HX1 as function of deformation frequency f in Hz. For the relaxation parameter To_3, a two step behaviour was found. Part one comprises 0.1 to 10 Hz and part two 10 Hz to 30 Hz.

quantity	**function type**	**equation**	**correlation coeff. R^2**
A_1 [°C]	logarithmic	$A_1 = 1.0844*\ln(f) + 11.813$	0.8827
A_2 [°C]	logarithmic	$A_2 = 1.0621*\ln(f) + 7.4516$	0.9781
A_3 [°C]	logarithmic	$A_3 = 1.2387*\ln(f) + 21.792$	0.9154
w_1 [°C]	logarithmic	$w_1 = 0.4470*\ln(f) + 4.7975$	0.9645
w_2 [°C]	logarithmic	$w_2 = 0.4734*\ln(f) + 3.6964$	0.9346
w_3 [°C]	logarithmic	$w_3 = 1.3434*\ln(f) + 26.408$	0.9655
Tc_1 [°C]	logarithmic	$Tc_1 = 1.8352*\ln(f) – 77.910$	0.9840
Tc_2 [°C]	logarithmic	$Tc_2 = 2.2024*\ln(f) – 71.792$	0.9271
Tc_3 [°C]	logarithmic	$Tc_3 = 3.7982*\ln(f) – 45.632$	0.9753
To_1 [°C]	linear	$To_1 = 0.0119*f + 0.84398$	0.7801
To_2 [°C]	linear	$To_2 = 0.1395*f + 11.607$	0.8709
To_3 [°C]	linear, part 1	$To_3 = 2.5848*f + 27.348$	0.9999
To_3 [°C]	linear, part 2	$To_3 = 0.2415*f + 50.792$	(1.00)

4.2 Modelling of the loss factor curve changed with ageing

The Figs 22 to 27 show the EMG modelling of the loss factor curves of unaged CRP1 and of two aged CRP1 samples with the following ageing conditions: 60°C, 75 days and 60°C, 220 days. The EMG descriptions change systematically with ageing as can be seen in Figs 25 to 27, where only the model curves are shown. For clearness, Figs 25 and 26 show only two sets of curves. The intensity of peak P3 decreases, the EMG maximum is shifted to lower intensity values of tanδ and its asymmetry is decreased, means To_3 becomes smaller. Peak P1 is changed only little in maximum temperature and intensity, see Table 12. Major changes are recognisable for peak P2. Its asymmetry and intensity increase. The maximum temperatures of the Gauss parts of the EMGs are more or less constant only a slight shift to lower temperatures is expressed. All parameters have been described as function of ageing. The results are compiled in Table 13 together with a note on the change. Of significant interest is also the behaviour of CRP in effect of ageing on the master curves of G' and G''. A recent work has discussed the effects [14]. It was necessary to generate sub-master curves, means below and above the main glass-rubber transition. Increasing age has less influence on higher deformation rates than on lower ones.

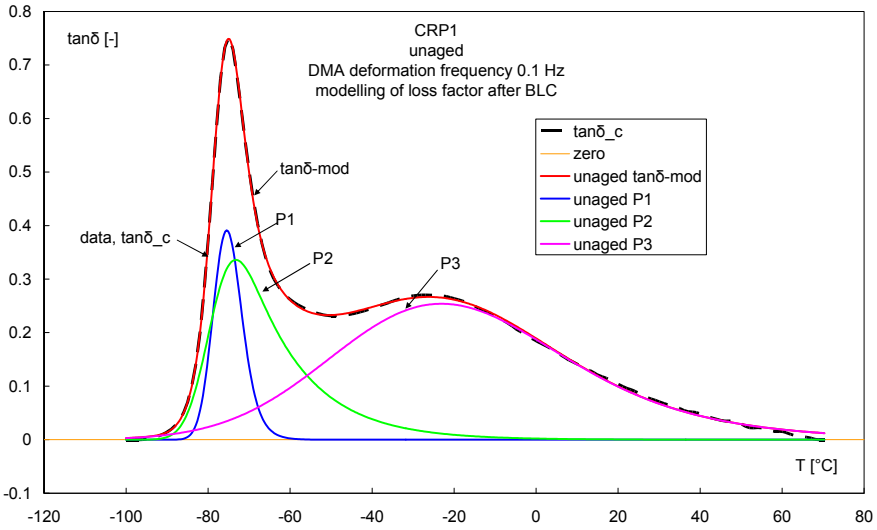

Figure 22: Description of the loss factor of the unaged CRP1 with three EMG functions at 0.1 Hz deformation frequency.

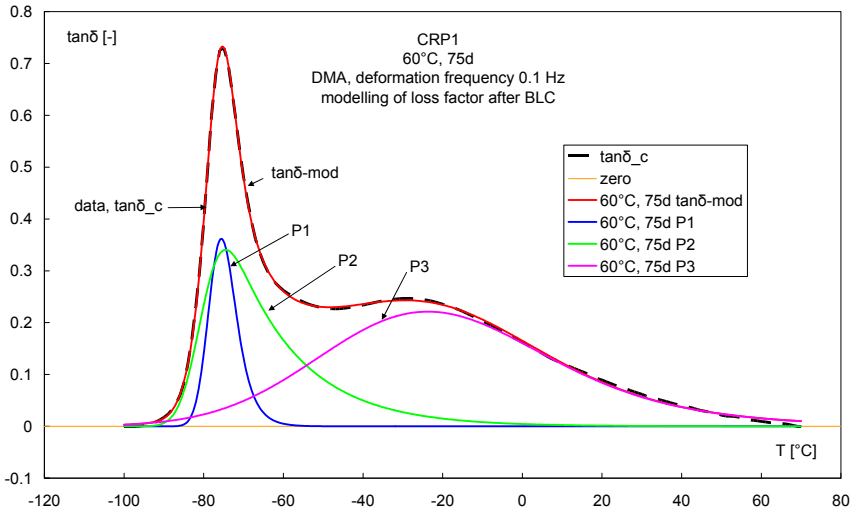

Figure 23: Description of the loss factor of the aged CRP1 (60°C, 75 days) with three EMG functions at 0.1 Hz deformation frequency.

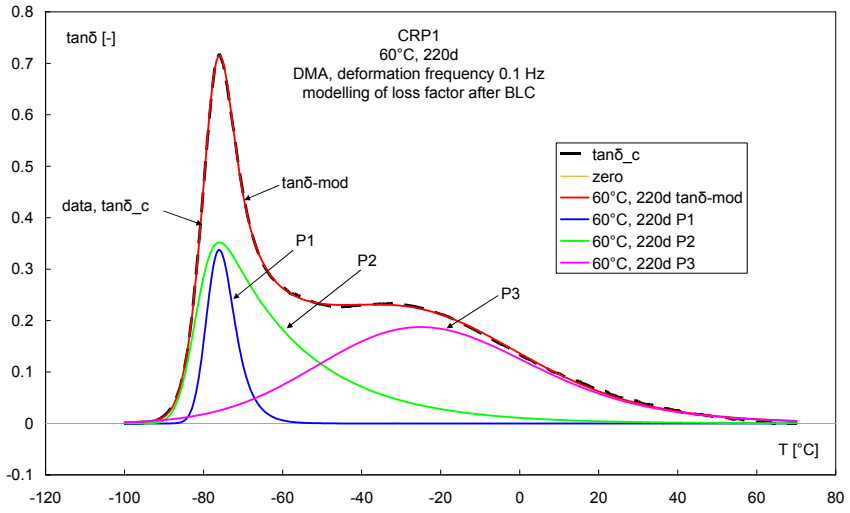

Figure 24: Description of the loss factor of the aged CRP1 (60°C, 220 days) with three EMG functions at 0.1 Hz deformation frequency.

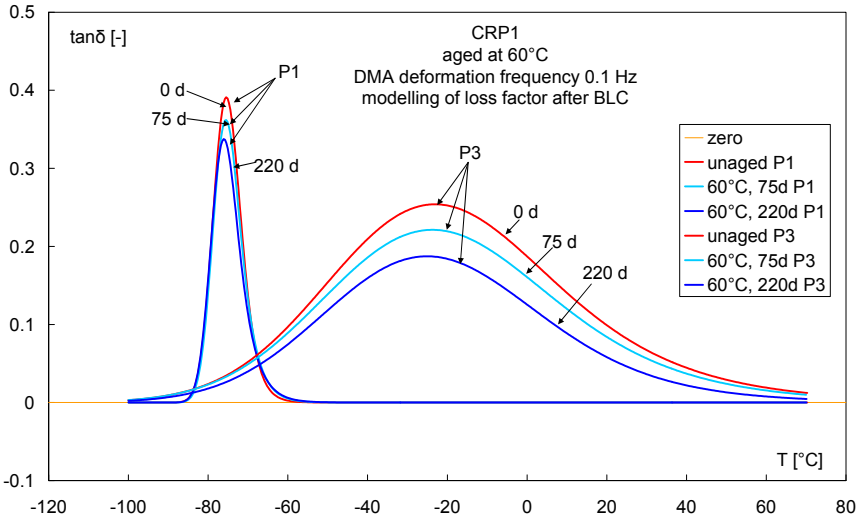

Figure 25: Modelling parts of the peaks P1 and P3 of CRP1 at 0.1 Hz deformation frequency.

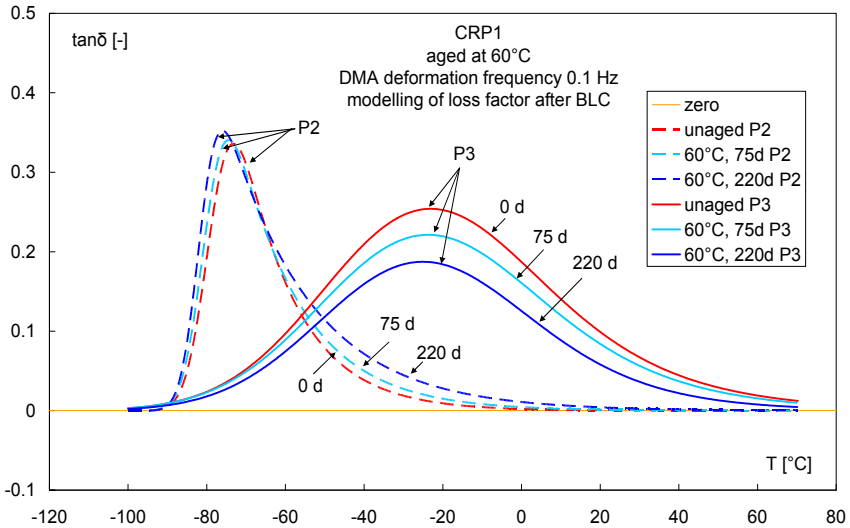

Figure 26: Modelling parts of the peaks P2 and P3 of CRP1 at 0.1 Hz deformation frequency.

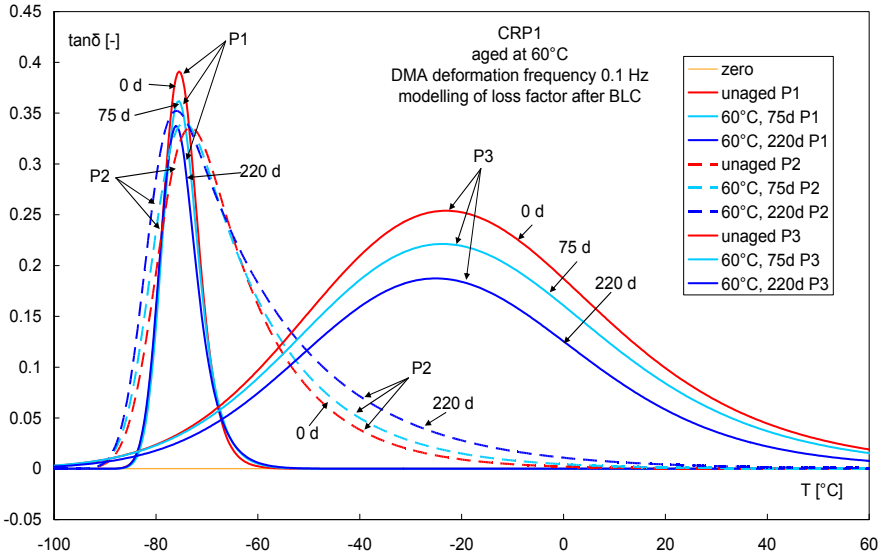

Figure 27: Modelling parts of the peaks P1, P2 and P3 of CRP1 at 0.1 Hz deformation frequency.

Table 12: EMG fit parameters of the loss factor curves of CRP1 as function of ageing at 60°C in days. The column 'change' gives the ratio of values between the aged state at 60°C, 220 days and the unaged state. Significant changes occur with A_2, A_3 To_2 and To_3. All others parameters are only slightly ageing dependent.

quantity	unaged	60°C, 75d	60°C, 220d	change	trend with ageing
td_0	0	0	0	0	
A_1 [°C]	3.527 ± 0.5	3.329 ± 0.3	3.176 ± 0.3	0.90	nearly constant
A_2 [°C]	8.242 ± 0.4	9.050 ± 0.3	10.615 ± 0.4	1.29	increase
A_3 [°C]	18.993 ± 0.4	16.576 ± 0.5	13.113 ± 0.6	0.69	decrease
$\sum A_i$ [°C]	30.76 ± 0.4	28.96 ± 0.4	26.9 ± 0.4	0.87	-
w_1 [°C]	2.993 ± 0.2	2.8056 ± 0.1	2.7388 ± 0.1	0.92	nearly constant
w_2 [°C]	4.7107 ± 0.5	4.3632 ± 0.3	3.7606 ± 0.2	0.80	nearly constant
w_3 [°C]	23.419 ± 0.5	23.784 ± 0.5	23.137 ± 0.5	0.99	nearly constant
Tc_1 [°C]	-77.262 ± 0.2	-77.612 ± 0.2	-78.216 ± 0.2	1.01	nearly constant
Tc_2 [°C]	-78.922 ± 0.6	-80.281 ± 0.4	-81.725 ± 0.3	1.04	nearly constant
Tc_3 [°C]	-39.377 ± 0.7	-39.814 ± 0.8	-39.262 ± 0.8	1.0	nearly constant
To_1 [°C]	2.4134 ± 0.4	3.0389 ± 0.4	3.4007 ± 0.3	1.41	medium increase
To_2 [°C]	13.961 ± 1.4	16.631 ± 1.7	21.305 ± 2.1	1.53	increase
To_3 [°C]	23.337 ± 0.6	22.633 ± 0.6	18.959 ± 0.6	0.81	decrease
SD^2	2 E-05	1 E-05	7.9 E-06	-	-
R^2	0.99942	0.9995	0.99969	-	-

Table 13: EMG fit parameters of the loss factor curves of CRP1 as function of ageing time at 60°C. All four fit parameters can be described with a linear trend with ageing time in the load range applied. Time t is in days.

quantity	function type	equation	correlation coeff. R^2	trend with ageing
A_1 [°C]	linear	A_1 =-1.708 E-03 * t + 3.5274	0.9124	nearly constant
A_2 [°C]	linear	A_2 = 1.079 E-02 * t + 8.2420	1.0000	increase
A_3 [°C]	linear	A_3 =-2.730 E-02 * t + 18.993	0.9913	decrease

w_1 [°C]	linear	w_1 =-1.297 E-03 * t + 2.9933	0.7379	nearly constant
w_2 [°C]	linear	w_2 =-4.351 E-03 * t + 4.7107	0.9989	nearly constant
w_3 [°C]	linear	w_3 =-6.417 E-04 * t + 23.419	0.9478	nearly constant
Tc_1 [°C]	linear	Tc_1 =-4.371 E-03 * t – 77.262	0.9988	nearly constant
Tc_2 [°C]	linear	Tc_2 =-1.330 E-02 * t – 78.922	0.9629	nearly constant
Tc_3 [°C]	linear	Tc_3 =-1.384 E-04 * t – 39.377	0.7650	nearly constant
To_1 [°C]	linear	To_1 = 4.889 E-03 * t + 2.4134	0.8501	medium increase
To_2 [°C]	linear	To_2 = 3.361 E-02 * t + 13.961	0.9991	increase
To_3 [°C]	linear	To_3 =-1.881 E-02 * t + 23.337	0.9496	decrease

5 Summary and conclusions

The loss factor tanδ obtained by DMA measurements contains important information on the mobility phases or fractions of the binder of elastomer bonded energetic materials. With the often used HTPB-IPDI-based binders the loss factor curve contains two apparent peak regions and therefore at least two mobility fractions of the binder exist. Glass-rubber transition temperatures Tg are here defined as the maximum temperatures of the maxima in the loss factor curve. A discussion of the main influences on the loss factor curve was given. Essential for low Tg values are the effects that increase the free volume for the chain motions and all features that reduce the interaction energies between the chains of the elastomer and the plasticiser. Because the binder GAP has a lot of polar groups in the polymer chain, which is also linear, the glass-rubber transition must be at higher temperature values compared to the HTPB binder, which has no polar groups and is non-linear. An estimation of intermolecular interaction energies between HTPB chains and GAP chains has been presented in [6].

The loss factor curve contains information about the transition from the energy elastic state to the entropy (rubber) elastic state by molecular rearrangement processes. These processes are affected by external impacts as strain, deformation rate and ageing. To extract the information about these processes and their dependence on these external impacts a modelling of the loss factor curve has to be achieved. Therefore a procedure has been worked out and is presented here. The loss factor is a normalized measure of the energy consumption needed to perform the molecular rearrangement processes. Also dissipation effects are contained. With filled elastomers the latter are expressed as an offset of the curve in the rubbery state. To eliminate the dissipative part, a baseline correction has to be applied on the loss factor curve. To do this a special iteration procedure was developed. The baseline corrected loss factor is subjected to a modelling with so-named exponentially modified Gauss (EMG) distribution functions in order to separate the different mobility fractions. Through the EMG modelling also the residual dissipative part in the curves can be taken into account. One EMG function is characterised by four parameters, which have to be determined: peak intensity A, half peak width w of the Gauss part, maximum temperature Tc of the Gauss part and the relaxation parameter To of the exponential part. The EMG modelling of the loss factor curves of HTPB-binders has revealed the presence of three transition regions or mobility fractions in the complete loss factor curve instead of only two, as it is evident from the shape structure of tanδ of HTPB-IPDI binders. These three regions seem to be typical for the HTBP-based binders also using other curing agents, because they were also found with several materials containing this binder type [9, 10]. By changing the experimental conditions such as deformation rate or ageing, it was found that the three mobility fractions for the HTPB-based materials belong to the: (i) mobility unrestricted binder fraction with the lowest glass-rubber transition temperature; (ii) mobility restricted binder fraction with intermediate glass-rubber transition temperature; (iii) hindered binder fraction or stronger mobility restricted fraction with the highest glass-rubber transition temperature. The intensity of the unrestricted binder fraction is only slightly influenced by the external impacts deformation

rate and ageing. The other two fractions show clearly a dependence on deformation rate and ageing effects, especially in intensity, peak broadness and relaxation parameter. The conclusion is that these two mobility parts reflect essential changes in the binder and in the binder-filler interaction with external impacts. The maximum temperature of the main peak in the loss factor curve is not enough as assessment quantity. Further work will elucidate the behaviour of the mobility fractions of HTPB-IPDI binders including investigations with small rocket motor configuration using embedded stress sensors [15]. Further on, one must state that with iron based burning catalysts for AP the ageing of CRP can be strongly affected.

6 Abbreviations

Al	aluminium, fuel
AP	ammonium perchlorate, oxidiser
BLC	baseline correction
CRP	composite rocket propellant, based on binder AP, Al
DMA	dynamic mechanical analysis
DOA	dioctyl adipate, plasticiser
DSC	dynamic scanning calorimetry
EMG	exponentially modified Gauss distribution
FPi	fit parameter i
GAP	glycidyl azide polymer (energetic binder), hydroxyl terminated
HEC	high explosive charge
HTPB	hydroxyl terminated polybutadiene, binder
HX	high explosive
IPDI	isophorone diisocyanate, curing agent for PUR elastomers
N100	Desmodur^{TM} N100, curing agent for PUR elastomers
N3400	Desmodur^{TM} N3400, curing agent for PUR elastomers
PBX	Polymer bonded explosive
PUR	Polyurethane, also PU
RP	rocket propellant
$Tg_{,DMA}$	Glass-rubber transition temperature defined as temperature at maximum of tanδ (loss factor) curve, determined by DMA
$Tg_{,DSC}$	Glass-rubber transition temperature defined as temperature of the half height in the step of the change of specific heat c_P during the transition, determined by DSC
MAP	mobile amorphous phase
MAF	mobile amorphous fraction
RAP	rigid amorphous phase
RAF	rigid amorphous fraction
G'	storage shear modulus
dG'/dT	temperature derivative of G', to determine the temperature at maximum
G''	loss shear modulus
E'	storage tensile (Young) modulus
E''	loss tensile (Young) modulus
tanδ	loss factor, tanδ = G''/G' = E''/E'
tanδ_max1	main maximum of loss factor, unrestricted binder
tanδ_max2	second maximum of loss factor, hindered binder
δ	phase angle
α	normalised cumulative partition function of tanδ(T)
T	temperature

7 Acknowledgements

Our colleagues at Fraunhofer ICT, Dr. Klaus Menke (composite rocket propellants) and Dr. Peter Gerber (high explosive charges) are thanked for the careful manufacturing of the formulations and for providing information about the ingredients.

The 'Center for Energetic Concepts Development' (CECD) of University of Maryland, College Park, MD 20742, USA, http://www.cecd.umd.edu/ is thanked for the possibility to publish this present paper as an additional version to the publication in CALCE EPSC Press [11].

8 References

[1] Cerri, S. Bohn, M.A., Menke, K., Galfetti, L. (2010) Ageing of HTPB/Al/AP rocket propellant formulations investigated by DMA measurements, Sol-Gel and GPC Analysis. Paper 42, pp. 42-1 to 42-38 in *Proc. of 41st International Annual Conference of ICT on 'Energetic Materials',* Karlsruhe, Germany. ISSN 0722-4087. June 29 to July 2, **2010.**

[2] Cerri, S. Bohn, M.A., Menke, K., Galfetti, L. Ageing Behaviour of HTPB Based Rocket Propellant Formulations. *Central European Journal of Energetic Materials,* 6(2), pp. 149-165, **2009**.

[3] Cerri, S. Bohn, M.A., Ageing of HTPB/AP/Al rocket propellant formulations investigated by Dynamic Mechanical Analysis and Sol-Gel Analysis. *Proc. of 13th Seminar on 'New Trends in Research of Energetic Materials',* pp. 57 – 88. University of Pardubice, Pardubice, Czech Republic. April 21-23, **2010**.

[4] Cerri, S. *Characterisation of the ageing of advanced solid rocket propellants and first step design of green propellants.* PhD thesis, Politecnico di Milano, Dipartimento di Energia, Via Lambruschini 4, I-20156 Milano. Dottorato di Ricerca in Energetica, XXII ciclo, March **2011**.

[5] Cerri, S., Bohn, M.A., Menke, K., Galfetti, L., Ageing of HTPB/Al/AP rocket propellant formulations investigated by DMA measurements. *Propellants Explosives Pyrotechnics*, 38(2) pp. 190-198, **2012**.

[6] Bohn, M.A., Cerri, S,. Molecular mobility in binder systems. *Proc. of the 42nd International Annual Conference of ICT on 'Energetic Materials',* Version CD-Proceedings, pp. 96-1 to 96-3. Karlsruhe, Germany. ISSN 0722-4087. 3 June 28 to July 1, **2011**.

[7] Bohn, M.A., Evangelisti, C., Klapötke, Th.M., Atomistic simulation of the temperature dependence of density and van-der-Waals interactions of binders, plasticizers and mixtures of them. *Proc. of the 45th International Annual Conference of ICT on 'Energetic Materials – Particles, Processing, Applications'* Paper 114, pages 114-1 to 114-18. Karlsruhe, Germany. ISSN 0722-4087. June 24 to 27, **2014**.

[8] Nardai' M.M., Bohn, M.A., Wetting of Oxidizer Particles by Binder and Plasticizer Molecules - Microcalorimetry Experiments and Computer Simulations. *Proc. of 18th Seminar on 'New Trends in Research of Energetic Materials'*. University of Pardubice, Pardubice, Czech Republic. April 15-17, **2015**.

[9] Seyidoglu, T., Bohn, M.A., Effect of curing agents and plasticizers on the loss factor curves of HTPB-binders quantified by modelling. *Proc. of 18th Seminar on 'New Trends in Research of Energetic Materials'*. University of Pardubice, Pardubice, Czech Republic. April 15-17, **2015**.

[10] Ferrapontoff Lemos, M., Bohn, M.A., Evaluation of the effect of plasticizers on the DMA loss factor, the thermal and mechanical properties of Desmophen® 2200 based elastomers used for composite propellants. *Proc. of 18th Seminar on 'New Trends in Research of Energetic Materials'*. University of Pardubice, Pardubice, Czech Republic. April 15-17, **2015**.

[11] Tsagaropoulos, G., Eisenberg, A., Dynamic Mechanical Study of the Factors Affecting the Two Glass Transition Behavior of Filled Polymers. Similarities and Differences with Random Ionomers. *Macromolecules,* 28, pp. 6067-6077, **1995**.

[12] Programme package ,Origin' Version 7.0 (German), SR 4, v7.0552. Data Analysis and Graphing Software. OriginLab Corporation, One Round House Plaza, Suite 303, Northhampton, MA 01060, USA.

[13] Bohn, M.A., Impacts on the loss factor curve and quantification of molecular rearrangement regions from it in elastomer bonded energetic formulations. Chapter 10 (pp 195-235) in R. Armstrong, J. Short, D.K. Anand, eds. '*Energetics Science & Technology in Central Europe*'. CALCE EPSC Press, University of Maryland, College Park, MD 20742, USA, **2012**.

[14] Mußbach G., Bohn M.A., Influence of isothermal ageing on the mechanical properties of HTPB-bonded composite rocket propellants expressed as master curves of torsion DMA measurements. *Proc. of the 45th International Annual Conference of ICT on 'Energetic Materials – Particles, Processing, Applications'* Paper 114, pages 103-1 to 103-11. Karlsruhe, Germany. ISSN 0722-4087. June 24 to 27, **2014.**

[15] Mußbach G., Bohn M.A., Monitoring of bondline-stresses in case-bonded composite rocket propellant. *Proc. of 18th Seminar on 'New Trends in Research of Energetic Materials'*. University of Pardubice, Pardubice, Czech Republic. April 15-17, **2015**.